

Design and validation of clamping system for Wire and Arc Additive Manufacturing Internship report

Author: Manuel Veugelers
s1318152

Tecnalia supervisor: Dr. ir. M. Seco
UT supervisor: Prof. dr. ir. A. de Boer

Tecnalia research and innovation
Department of Industry and Transport
20009 San Sebastian
Spain

University of Twente
Faculty of Engineering Technology
Department Mechanics of Solids, Surfaces and Systems
P.O. Box 217
7500 AE Enschede
The Netherlands

April 12, 2018

UNIVERSITY OF TWENTE.

tecnalia  Inspiring
Business

Abstract

Wire and Arc Additive Manufacturing (WAAM) is an upcoming additive layer manufacturing technology that uses an electric plasma arc as heat source to melt and deposit wire-fed metallic material. High deposition rates and cost effectiveness make this technology a promising alternative to conventional machining. Today, one of the main challenges is the residual thermal stress causing distortions in the final product. An innovative clamping system has been designed to mitigate these distortions. A fully coupled thermo-mechanical finite element method (FEM) analysis is carried out to gain insight in the process and material behaviour, and to determine the occurring reaction forces in a simply constrained test set-up. These results, in combination with a static structural FEM analysis of the developed concept, resulted in a dimensioned clamping system. Validating analyses showed that the system behaves as expected and can withstand the loads that occur during the process. From this, an expandable modular clamping system is proposed, which is developed for a test set-up, but is applicable in the general case. Practical tests need to be performed to further validate the solution, which are planned to be carried out at the WAAM set-up at Tecnia. However, these tests fall outside the scope of this report.

Keywords: WAAM, additive manufacturing, clamping design, distortion, Finite element method (FEM)

Contents

1	Introduction	1
2	Background	3
2.1	Problem definition	3
2.2	Previous research	3
3	Design	6
3.1	Concepts	6
3.2	Concept choice	8
3.3	Final concept	9
4	Structural analysis	14
4.1	Thermo-mechanical analysis (estimation)	14
4.2	Static structural analysis (estimation)	17
4.3	Thermo-mechanical analysis (validation)	19
4.4	Static structural analysis (validation)	25
5	Redesign	28
5.1	Design	28
5.2	Validation	29
5.3	Actuators	30
6	Conclusion	32
6.1	Future work	32
	Bibliography	33
	Appendix A Material properties	35
A.1	Ti6Al4V	35
A.2	Stainless steel	36
	Appendix B Technical drawings	38
	Appendix C Screw jack datasheet	45

Chapter 1

Introduction

Tecnalia research and innovation is a private technological research institution based in San Sebastian, Spain. It provides research, technological development and innovation in the fields of sustainable construction, energy and environment, ICT, industry and transport, and health. Within the department of industry and transport, Tecnalia is currently engaged in additive manufacturing (AM), an increasingly popular and promising manufacturing technique enabling complex shaped parts. In an AM process, a product is built up by adding layers of material on top of each other. Usually, a digitally created model of the final product (CAD) is converted into paths for the manufacturing process (CAM). There are many methods of additive manufacturing, differentiating in their methods of material supply and deposition.

Wire and Arc Additive Manufacturing (WAAM) is one of the additive manufacturing methods researched and used at Tecnalia. With this method an electric plasma arc is used to melt the metallic feed material, which is supplied in wire form. An inert shielding gas is used for protection against oxidation. This process is similar to robotic TIG welding. In figure 1.1, a typical experimental set-up for a WAAM process is shown. With WAAM, relatively large metal products can be manufactured compared to alternative methods like laser cladding. High deposition rates can be achieved [1] and the only limits in size are the used welding torch manipulator and the protective gas environment. WAAM is a relatively new manufacturing technique, but it has great potential due to low production time, material efficiency and cost.

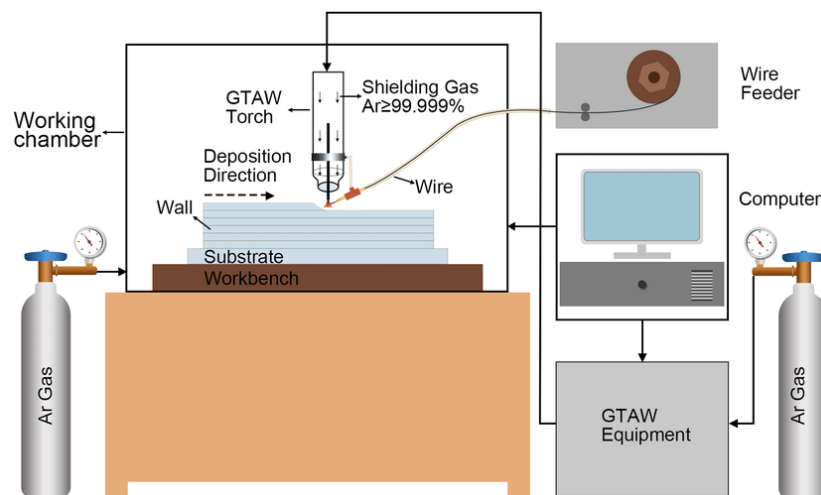


Figure 1.1: Typical experimental set-up for Wire and Arc Additive Manufacturing [2]

At Tecnia, a 5 axis gantry machine is used for the torch manipulation, which is developed in-house. Because highly reactive Titanium alloys are used in the process, a protective environment is implemented. In figure 1.2 the equipment used at Tecnia is shown. Figure 1.2C gives an example of a product which is manufactured by WAAM.

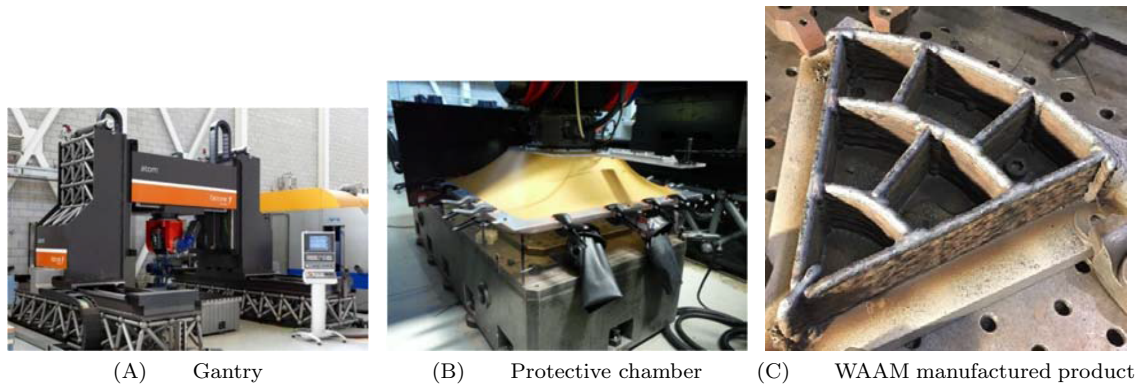


Figure 1.2: Wire and Arc Additive Manufacturing at Tecnia [3]

One of the main challenges at the moment is the prevention of distortions in the final product, as a result of residual thermal stresses. Research within Tecnia has shown that the way in which the workpiece is constrained during the process, is an important factor in the prevention of these distortions [4]. For that reason, a universal clamping system needs to be designed, which constrains the workpiece during material addition and does not require significant changes in product design.

In this report, the process of design and validation of such a clamping system will be described. First, a background of the problem will be given and previous research will be explained. After that, the design process will be described, resulting in the clamp design. The design will be supported by finite element method (FEM) simulations and this method will also be used to validate the final solution. Finally, conclusions will be given about the work and the results will be placed in the perspective of future work.

Chapter 2

Background

2.1 Problem definition

During the process of layer addition, the welding cycles cause non-uniform thermal expansion in the material. This causes residual stresses in the product, resulting in distortions. In figure 2.1, an example of such distortions in a product manufactured by WAAM is given. This simple part has been constrained using screws fixing the substrate plate to the baseplate.



Figure 2.1: Distortions in a product manufactured by WAAM within Tecnia (source: internal Tecnia documentation)

Distortions like this are currently the main issue in the production of proper industrial parts. In order to use the WAAM process commercially, thermal distortions and residual stresses in the final product need to be minimized.

2.2 Previous research

2.2.1 Sensitivity study

In order to understand the thermo-mechanical behaviour during WAAM manufacturing, a qualitative sensitive study is carried out within Tecnia [4]. In this study, a simple 200x200x10mm baseplate is considered, on which a 100mm high multi-layer wall is built. In figure 2.2, the model geometry is shown. With this simple model, a fully coupled thermo-mechanical finite element analysis is carried out.

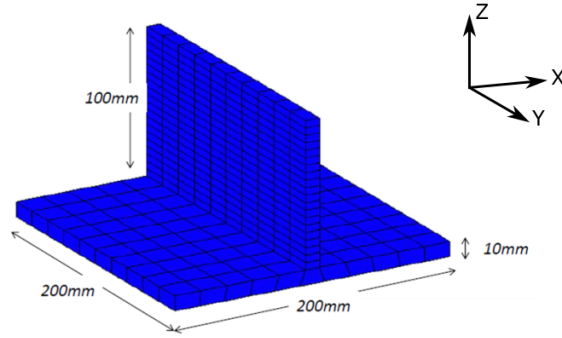


Figure 2.2: Geometry and dimensions of the simple WAAM test model

By means of 58 jobs, several relevant process parameters are analysed. In the simulations, simplifications are made in order to reduce computational time, but all simulations are argued to be affected the same way by this. As a qualitative analysis is conducted, the quantitative outcomes are therefore not relevant and the conclusions are considered to be correct. The parameters which are analysed in the study are:

- Clamping system: several methods of clamping are analysed
 1. Screws: this is the conventional way of clamping. It is simulated by constraining 6 nodes, corresponding to the screw locations.
 2. Fixed: all bottom nodes are fixed. Note that in reality this can never be achieved.
 3. Unconstrained
 4. Directionally constrained: free X or Y
- Preheating: several methods are analysed
 1. No preheating: this is the conventional way
 2. External: preheating before clamping
 3. In situ: preheating in clamped state
- Heat transfer to the table: either perfectly insulated or with a heat transfer coefficient
- Convection type: natural convection or forced convection for cooling
- Cooling down type: natural or controlled. In the controlled approach, the part is first heated to a uniform temperature, after which rapid cooling to room temperature is applied.

These parameters are combined alternatively in order to investigate the influence of each one on the process.

2.2.2 Results

The obtained results are presented in figure 2.3 in the form of relative distortions. It can be clearly seen that the used clamping system has a great influence on the results. Significant reductions in the distortions can be achieved if the right system is implemented. From figure 2.3A follows that generally more clamping results in less distortions. In the case that directional clamping is used, figure 2.3B shows that clamping in the direction of deposition gives the best results. Fixing the direction perpendicular to the deposition can even result in higher distortions than the totally fixed case. Since a clamping solution for the general case is required and no distinct deposition direction can be identified, the conclusion is maintained that more clamping is better.

Further improvements in the magnitude of the distortions can be achieved by preheating the substrate plate, as can be concluded from figure 2.3C. The best results are obtained if preheating is performed

before clamping. From figure 2.3D and 2.3E it becomes clear that during the process heat losses should be minimized. Therefore the table should be insulated and no forced convection should be used. The method of cooling does not have a significant influence on the final distortions, but figure 2.3F suggests that a controlled cooling stage might be beneficial.

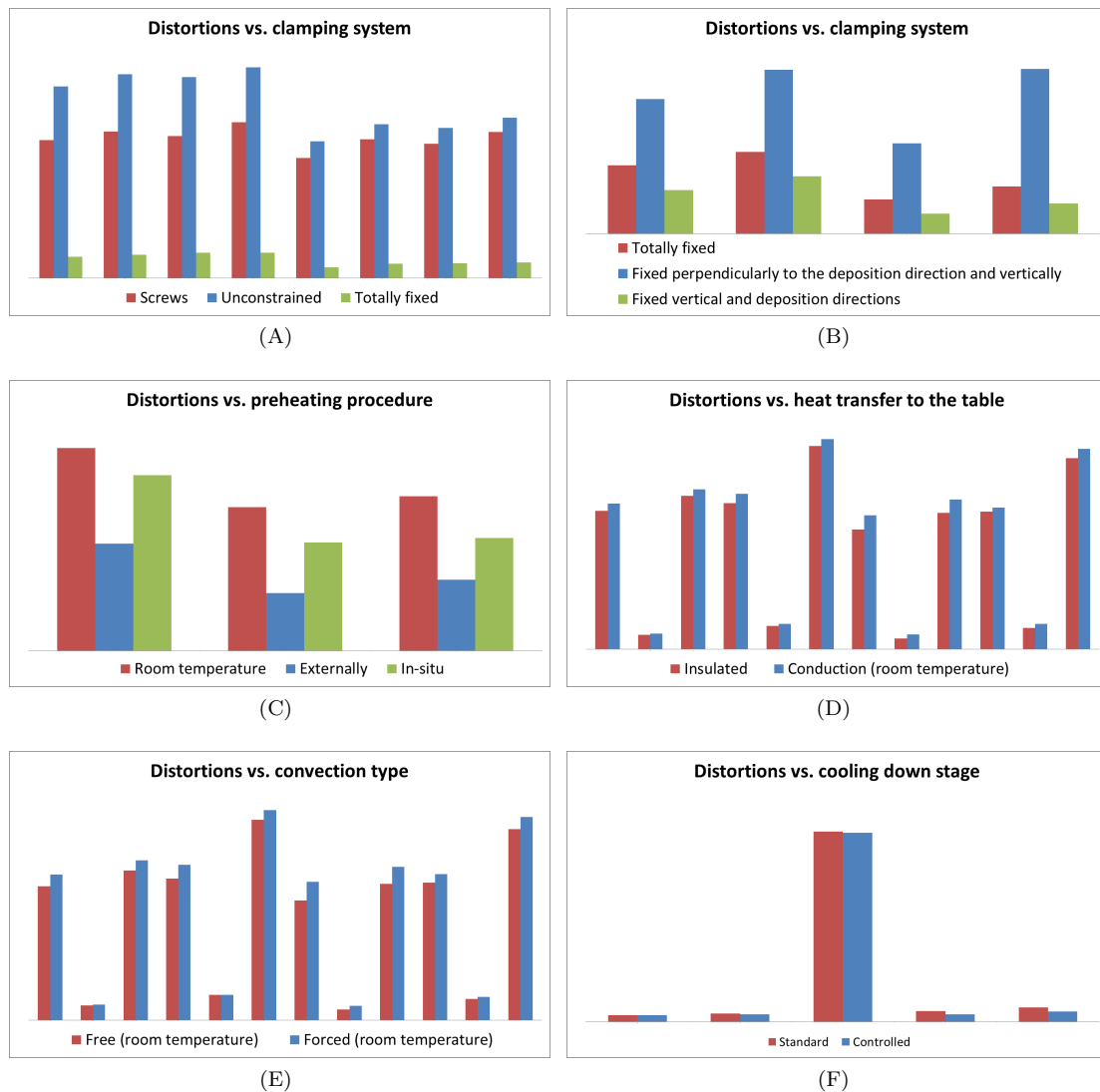


Figure 2.3: Qualitative job results of the sensitivity analysis [4]

In this report, the focus will be on the improvement of the process by means of a proper clamping system. Currently, parts manufactured at Tecnia are constrained at the substrate plate which is used as base for the material addition. For this purpose, either clamps from the side are used or screws. This way of clamping means that around the weldline there can be no constraints. From the above results can be concluded that this way of clamping is not sufficient, and significant improvement can be achieved. For that reason, the design of an innovative clamping system is proposed.

Chapter 3

Design

3.1 Concepts

Four concepts are developed, outlining principles to fix the workpiece plate to the rigid base.

3.1.1 Concept 1

The first concept is based on a form closed connection, which can be opened and closed for clamping. A dovetail shaped groove is constructed in the substrate plate. Using a certain mechanism, wedges are pushed from the inside onto the tapered edge of the dovetail, causing the plate to be clamped down to the base. The principle and derived concepts are shown in figure 3.1. Three variants are considered for the realisation of the mechanism: a piston, a worm wheel or a threaded rod. A piston makes use of a pressure difference and can either be hydraulic or pneumatic. A mechanical alternative for this is the worm plus wheel connection. As the worm gear rotates with the worm, the inner rod is translated, as shown in figure 3.1C. Another mechanical alternative is the threaded rod as shown in figure 3.1D, which uses one single rod to drive all wedges. Note that the thread direction has to alternate along the rod for this.

3.1.2 Concept 2

Concept 2 is based on the principle of inserting an expandable object into a similar dovetail shaped groove or holes as concept 1. The main difference is that a smaller width of the groove is sufficient. After expansion of the inserted object, tension is applied from the bottom side to clamp the workpiece. The principle and derived concepts are shown in figure 3.2. The two options considered are (an adaptation of) a toggle bolt or an expansion bolt. The first one includes two extensions that expand using a spring, resembling a butterfly motion. The second one uses a conical nut to deform the bolt. In both cases, removal of the insert is not trivial.

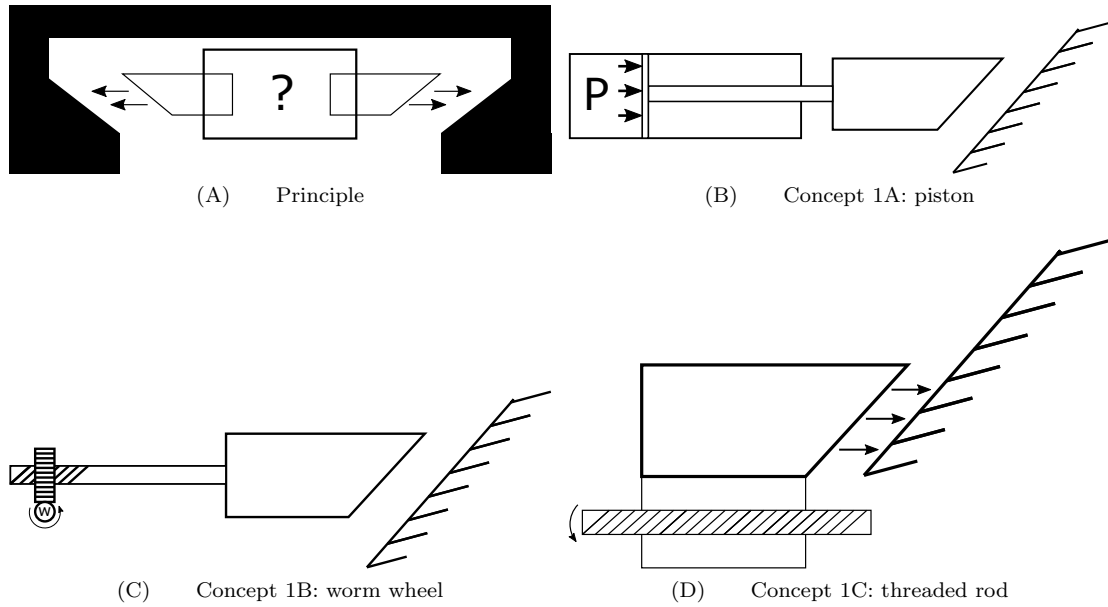


Figure 3.1: Concept 1

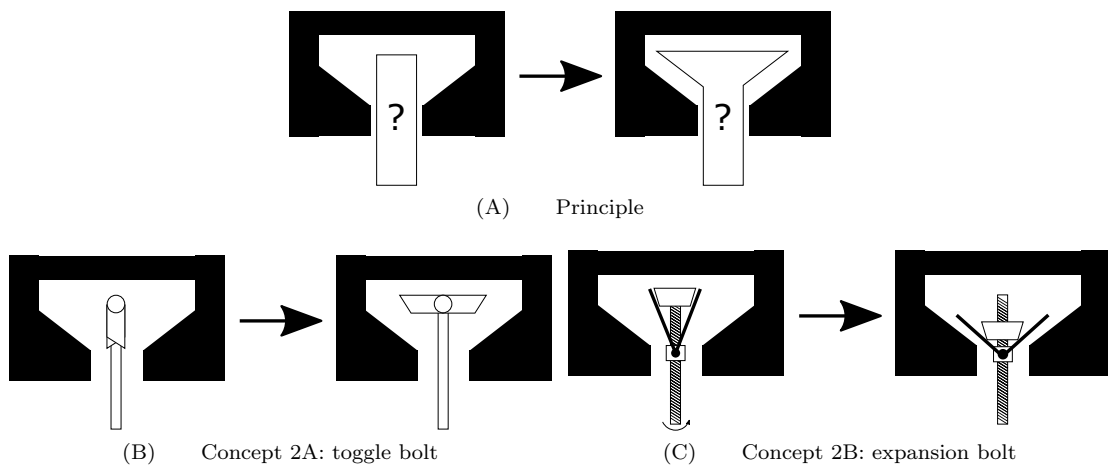


Figure 3.2: Concept 2

3.1.3 Concept 3

Concept 3 uses one or more vacuum zones to fix the plate to its position, as shown in figure 3.3. Because of the pressure difference between vacuum and atmospheric pressure, the maximum force on a standard 200x200mm plate is limited:

$$\Delta P = 1\text{bar} = 1 \cdot 10^5 \text{Pa} \quad (3.1)$$

$$A = 0.2 \cdot 0.2 = 0.04\text{m}^2 \quad (3.2)$$

$$F_{max} = A\Delta P = 4\text{kN} \quad (3.3)$$

Using the standard plate with a 10mm thickness, test within Tecnalia have shown that reaction forces in the order of magnitude of 28kN occur. This means that only (relatively) thin plates are suitable for this method, since the reaction forces resulting from the thermal distortion of thicker plates are too large.

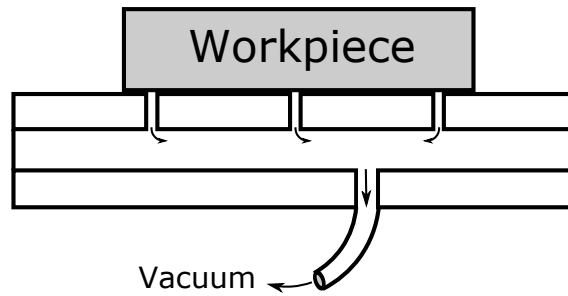


Figure 3.3: Concept 3: vacuum

3.1.4 Concept 4

The fourth and final concept is based on the use of pure friction for restraining the workpiece. It is based on the principle of concept 1, but does not include a form closed connection. This results in a plate geometry which is easier to machine than the dovetail structures. However, significant forces are required to provide sufficient friction for the clamping.

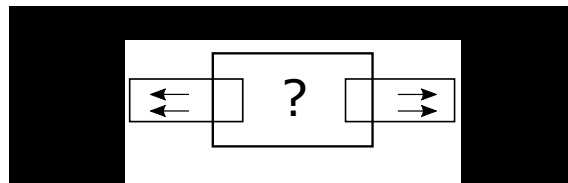


Figure 3.4: Concept 4: frictional clamping

3.2 Concept choice

Based on the concepts presented in section 3.1 a motivated choice is made for the concept which will be further developed. In table 3.1 the advantages and disadvantages to each concept are listed. Based on this table, concept 3 and 4 are eliminated. Since customer demands may require the substrate plate to be a part of the final product, changes to the geometry of this plate are not desirable. Since vacuum forces are only large enough to clamp thin plates, concept 3 is not feasible for this specific situation. Concept 4 is eliminated because of the large forces that occur during the process. It is reasoned to be more effective to add some thickness to the plate for geometrical constraint than to significantly increase the clamping forces.

After internal discussion within Tecnalia, concept 1 is chosen to be detailed further. The dovetail shape is considered the most convenient method to form constrain the plate, while minimizing necessary machining operations. A pressure based actuator is preferred above the other concept variants because of the possibility to distribute the force evenly over the actuators, but other actuation methods will be considered as well.

Concept	Advantage	Disadvantage
1A: piston	- Pressure distributed over all clamping elements - Large clamping force	- Expensive - Availability small size
1B: worm wheel	- Large gear ratio → large clamping force	- Complex
1C: threaded rod	- Simple	- Difficult to distribute force
2A: toggle bolt	- Easy installation - No base structure needed, just insertable pieces	- Not very robust - Difficult to remove
2B: expansion bolt	- Easy installation - No base structure needed, just insertable pieces	- Difficult to remove
3: vacuum	- No machined structures are needed in the plate - Thick plate not necessary	- Only suitable for relatively thin plates - Difficult to insulate (choice of material)
4: frictional clamping	- No undercut necessary, easier to manufacture	- Larger clamping force necessary

Table 3.1: Advantages and disadvantages of the concepts

3.3 Final concept

3.3.1 Estimating calculations

An important parameter of the final design is the total thickness of the substrate plate, as material costs should be minimized as much is possible. Therefore it is useful to know the additional thickness needed for the dovetail geometry. The determining factor in that is the ridge of the dovetail where the clamping force is applied, marked A in figure 3.5.

For the purpose of the calculations, the ridge is modelled as a clamped beam with rectangular cross



Figure 3.5: Substrate plate with dovetail ridge marked A

section. Some initial values are chosen:

$$a = 0.2m \quad (\text{the complete width of the substrate plate}) \quad (3.4)$$

$$b = 0.01m \quad (\text{the length of the ridge, arbitrarily chosen realistic value}) \quad (3.5)$$

$$t = ? \quad (\text{variable thickness, unknown}) \quad (3.6)$$

$$F_{max} = 28kN \quad (\text{maximum occurring reaction force during earlier FEM simulations}) \quad (3.7)$$

$$\sigma_y = 250MPa \quad (\text{yield strength of structural steel}) \quad (3.8)$$

Beam theory

First, the ridge of the dovetail is considered as a simple clamped beam under bending load by a force F_{max} at the end of the beam. The maximum internal bending moment M then occurs at the clamped end of the beam and is given by:

$$M = F_{max}b \quad (3.9)$$

The bending stress at a arbitrary distance y from the neutral axis is given by[5]:

$$\sigma_{bend} = \frac{My}{I} \quad (3.10)$$

In this, I is the moment of inertia of the cross section. For the considered rectangular cross section this is given by $I = \frac{at^3}{12}$. The maximum bending stress of the rectangular beam occurs at the maximum distance $c = \frac{1}{2}t$ from the neutral axis:

$$\sigma_{bend,max} = \frac{Mc}{I} \quad (3.11)$$

Equating equation (3.11) to the yield stress σ_y and solving for t yields:

$$t_{beam} = 5.8mm \quad (3.12)$$

Plate theory

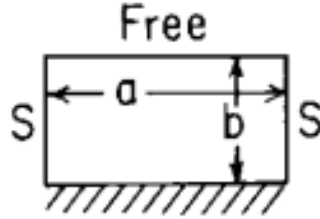


Figure 3.6: Schematic drawing of the boundary conditions of the dovetail ridge, using plate theory [6]

Next, the ridge of the dovetail is considered as a rectangular plate which is clamped at one edge, free at the opposite edge and simply supported at the remaining edges, as shown in figure 3.6. The plate is loaded by a uniform pressure P given by:

$$P = \frac{F_{max}}{ab} \quad (3.13)$$

According to Roark's formulas for rectangular plates [6], the maximum stress at the midpoint of the fixed edge is given by:

$$\sigma_{max} = \frac{-\beta_1 P b^2}{t^2} \quad (3.14)$$

In this, β_1 is a coefficient obtained from tabular data [6]. Equating equation (3.14) to the yield stress σ_y and solving for t yields:

$$t_{plate} = 3.7mm \quad (3.15)$$

Conclusion

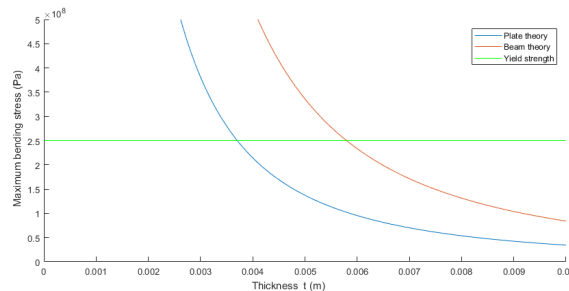


Figure 3.7: Maximum bending stress as function of the thickness t of the dovetail ridge

In figure 3.7 the maximum bending stress as function of the thickness of the ridge is shown for both beam and plate theory. In reality, the dovetail ridge is neither a beam or a plate, so an appropriate value for t will be somewhere in between the values of (3.12) and (3.15). An initial value of 5mm is chosen, which results in the global geometry as shown in figure 3.8.

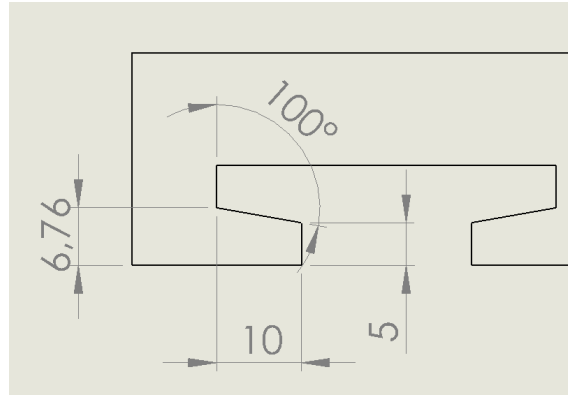


Figure 3.8: Initial chosen dimensions of the dovetail

3.3.2 Geometry

In the final concept, the choice is made to include a mirrored version of the dovetail groove in the baseplate in order to wedge-clip the two ridges together. Because of the limited space between the dovetails, a mechanism is constructed such that the motion of the cylinder acts in vertical direction. The final design is shown in figure 3.9. In the following section, the different parts of the assembly will be explained. Note that the plate geometry is divided into 9 sections in order to distribute the clamping force evenly.

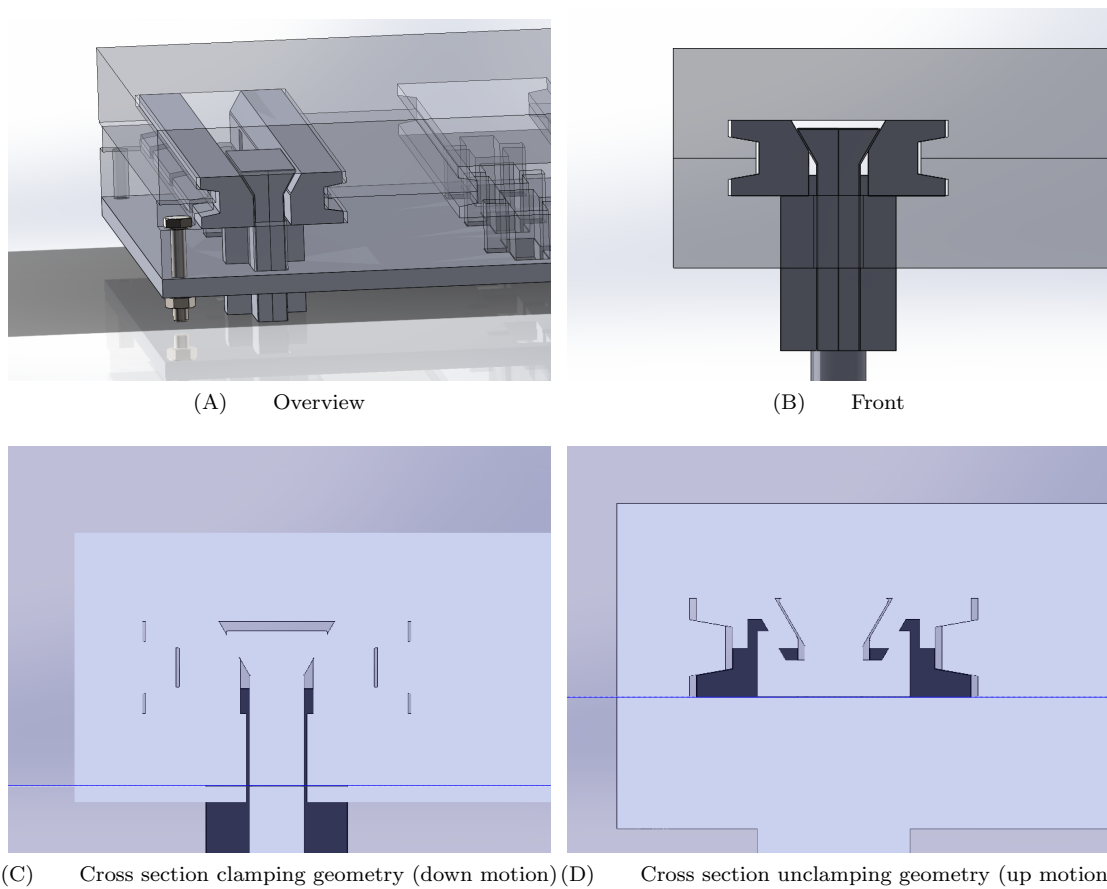


Figure 3.9: Final concept

Wedge

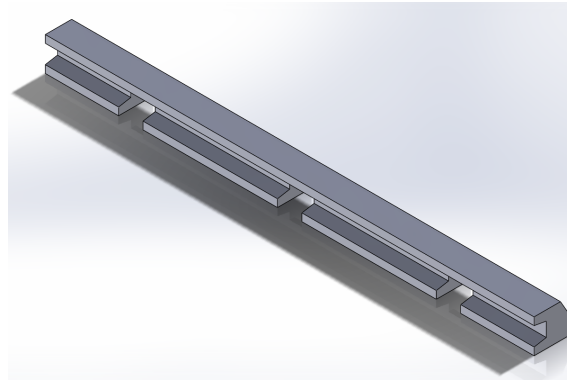


Figure 3.10: Model of the wedge

In figure 3.10 a model of the wedge part is shown. These parts are used to wedge-clip the dovetail ridges against each other. The distance between the two wedge parts is 0.2 mm smaller than the corresponding negative geometry of the two plates, such that clamping is possible. On the other side of the wedge is an edge with an angle of 45 degrees, which is used by the piston to push the two wedges to the outside with a downward motion, as shown in figure 3.9C. On the bottom inside of the wedge, angled grooves are added locally. This groove is used by protrusions in the piston to push the two wedges inside for unclamping, with an upwards motion of the piston. This is shown in figure 3.9D.

Piston

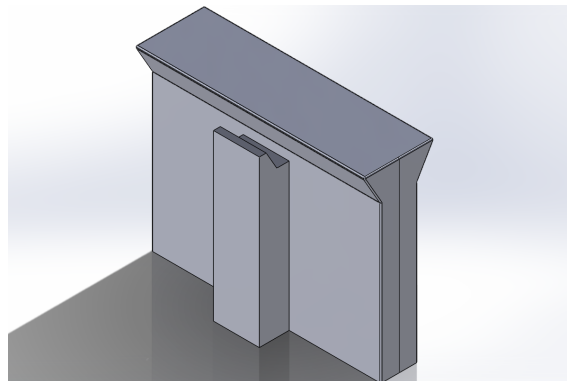


Figure 3.11: Model of the piston part

In figure 3.11 a model of the piston part is shown. The upper prismatic part is used to push the wedge parts outside, while the wider middle part is used to push the wedges back inside, as explained in the previous section. It is a complex part, so it might be necessary to manufacture it out of two or more parts. This can also be combined with the addition of insulation, since it was concluded during the parameter study [4] that the preheated baseplate and substrate need to be insulated during the addition process.

Baseplate

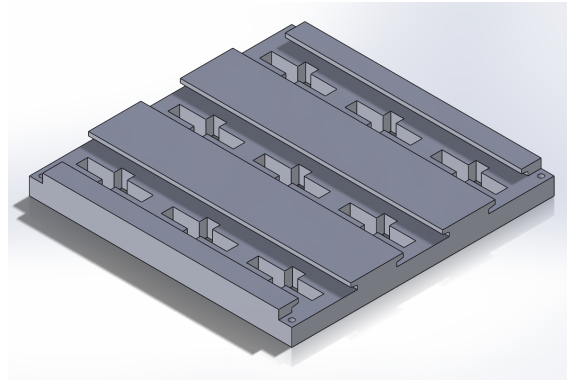


Figure 3.12: Model of the baseplate

In figure 3.12 a model of the baseplate part is shown. To accommodate for the geometry of the piston parts, cross-shaped holes are included inside the dovetail grooves. In the corners of the plate, holes are drilled for the connection between the baseplate and an insulation plate, as shown in figure 3.9A.

3.3.3 Actuators

For the actuation of the clamping cylinder, three options are considered: hydraulic, pneumatic and electro-mechanical. In table 3.2 the advantages and disadvantages of each option are listed.

	Advantages	Disadvantages
Hydraulic	<ul style="list-style-type: none">- high forces- low footprint at work point- easy to expand number of cylinders	<ul style="list-style-type: none">- large hydraulic power unit required- possible leakage- expensive
Pneumatic	<ul style="list-style-type: none">- high velocity- pneumatic system is already present- low maintenance	<ul style="list-style-type: none">- actuator size for large forces- pressure loss
Electro-mechanical	<ul style="list-style-type: none">- high precision- actuators can be driven interconnected- self locking can be applied	<ul style="list-style-type: none">- often dedicated controllers necessary- possible overheating

Table 3.2: Advantages and disadvantages of hydraulic, pneumatic and electro-mechanical actuation

Considering the large reaction forces that result from the WAAM process, hydraulic actuators would be the first choice. However, the initial investment and necessary maintenance for such a system are not justified by the advantages. Instead, it would be convenient to choose for a pneumatic actuation system, since a internal pneumatic system is already present at Tecnia. Although this would be the cheapest and most preferential method, after a brief market research of pneumatic actuators it was concluded that actuators capable of delivering enough force are too large to incorporate in the design. For this reason, the choice is made use electro-mechanical actuators. They provide a good balance between high actuation force and cost, and have the additional advantage that they can be interconnected in series or parallel, using only one electrical motor. Furthermore, in most cases self locking can be applied, which means that no continuous actuator power is necessary.

The used actuator will be further specified after a qualitative structural analysis in chapter 4, in which the occurring forces in the design are identified.

Chapter 4

Structural analysis

In order to check the feasibility of the concept and to dimension the actuator for the occurring reaction forces, a structural analysis is required. Using Finite Elements Analysis (FEA), realistic dimensions will be estimated based on necessary clamping force and thermal induced reaction forces. A coupled thermo-mechanical analysis in MSC Marc/Mentat is used to determine the reaction forces that occur while constraining the workpiece. The maximum values of these reaction forces are subsequently used in a static structural analysis in ANSYS, where the geometry is optimized and an equivalent stiffness is determined. After that, a simplified representation of the resulting geometry is used in another coupled thermo-mechanical analysis in MSC Marc/Mentat, in order to check the validity of the used reaction forces and to determine the expected distortions in the final product. Finally, another static structural analysis in ANSYS is done to evaluate the expected loadcases for the final geometries of the structure.

4.1 Thermo-mechanical analysis (estimation)

As mentioned in section 2.2, thermo-mechanical analyses of the WAAM process have been done before within Tecnia, so a meshed model of the original workpiece plate already exists. Most of the model and simulations are initially left as they are, since it accurately describes the process of addition of the welding layers and all associated thermo-mechanical behaviour. As the analysis is done to determine the effects of the clamping situation, changes are made to the geometry around the boundary conditions and to the boundary conditions themselves.

4.1.1 Geometry

The geometry used for the thermo-mechanical analysis consists of a simple square substrate plate of 200x200x10 mm on which a multi-layer “wall” is built using WAAM. This corresponds with the test set-up being used by Tecnia, as mentioned in section 2.2. After the addition of each layer, a waiting time is implemented to allow the added material to cool down enough to bond with the base material. After addition is complete, the product is cooled down to room temperature before clamp release. The relevant parameters of this test set-up are given in table 4.1. The material properties of Ti6Al4V are temperature dependant, and are taken from literature [1]. The used values for the material properties of Ti6Al4V can be found in appendix A.1. The model is meshed using Siemens NX and imported in MSC Marc/Mentat. The resulting meshed geometry is shown in figure 4.1. In the actual simulations, only half of this model is used since the geometry is symmetric with respect to the mid-plane of the wall.

Plate dimensions:	200x200x10 mm
Layer thickness:	5 mm
Number of layers:	20
Material:	Ti6AL4V
Feed speed:	4 mm/s
Waiting time between layers:	50 s
Cooling time before release:	20,000 s

Table 4.1: Relevant parameters of the test setup which is modelled in MSC Marc/Mentat

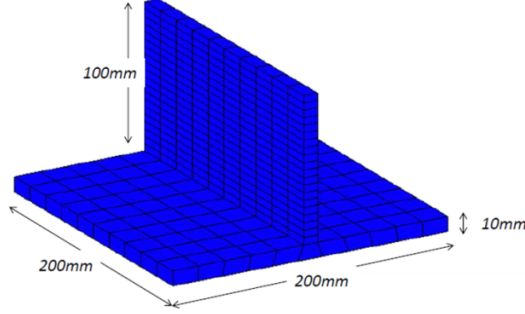


Figure 4.1: Meshed geometry and dimensions of the MSC Marc/Mentat model

4.1.2 Method and results

The WAAM process is simulated using the welding module of MSC Marc/Mentat, a finite elements software distribution specialised in analyses including non-linear effects like contact and thermal effects. A fully coupled transient thermo-mechanical analysis is carried out.

For the addition of material, two methods of simulation are considered: the quiet element method or the inactive element method (also called element birth technique) [7]. The quiet element method includes all elements from the start of the simulation, but scales the material properties of the “quiet” elements with a certain factor, such that they do not contribute significantly to the solution. The inactive element method creates the elements during the simulation. The first approach is chosen as it is easier to implement and the option is available in MSC Marc/Mentat.

The thermal effects of radiation and natural convection are captured using a face film boundary condition on the surface of the model. The contact with the table is assumed to be insulated, so the heat loss coefficient for conduction is set to zero. The heat source of the welding torch is modelled using a constant deposition temperature of 2000 degrees Celsius. This is the most simple and least computationally expensive method. It would be preferable in terms of accuracy to use a two dimensional Gaussian moving heat source, which describes the heat flux distribution q as function of the radial position r by [8]:

$$q(r) = \frac{\eta UI}{2\pi\sigma^2} e^{-(r^2/2\sigma^2)}, \quad (4.1)$$

where U and I are respectively the voltage and current of the welding arc, η is an efficiency coefficient, and σ is the radial distance. An even more accurate model is Goldak’s double ellipsoid distribution, which can be described by [9]:

$$q_f = \frac{6\sqrt{3}Qf_f}{\pi\sqrt{\pi}a_fbc} e^{\left[-3\left(\frac{x^2}{a_f^2} + \frac{y^2}{b^2} + \frac{z^2}{c^2}\right)\right]} \quad (\text{front quadrant}) \quad (4.2)$$

$$q_r = \frac{6\sqrt{3}Qf_r}{\pi\sqrt{\pi}a_rbc} e^{\left[-3\left(\frac{x^2}{a_r^2} + \frac{y^2}{b^2} + \frac{z^2}{c^2}\right)\right]} \quad (\text{rear quadrant}) \quad (4.3)$$

$$f_f + f_r = 2 \quad (\text{relation front and rear}) \quad (4.4)$$

In this, a_f and a_r are the length of the front and rear ellipsoid respectively, b is the width and c is the depth. Furthermore, Q is the total energy input and f_f and f_r are factors that distribute the power density over the front and the rear, while satisfying equation (4.4). Considering the necessary refined mesh to apply either of those methods and the resulting long calculation times, the more simple direct deposition temperature is reasoned to be sufficient for this case.

In order to modify the geometry to match the conceptual design of the clamping system, elements of the mesh corresponding to the locations of the three dovetail grooves are removed. The nodes inside the dovetail grooves are constrained in all directions, as shown in the red marked areas in figure 4.2. The

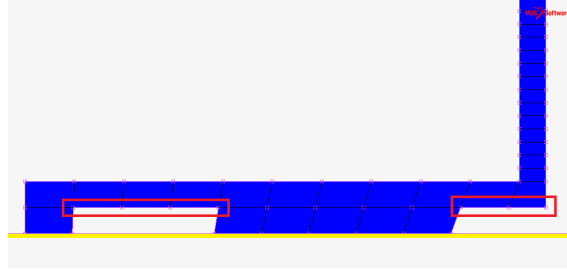


Figure 4.2: Side view of the MSC Marc/Mentat model, in which the constrained areas are marked red

usage of fixed constraints is considered a “worst case” scenario, since in reality there will always be some amount of stiffness in the structure which causes small deflections under load. As a result, the calculated reaction forces in the nodes will be higher than in reality. This inaccuracy is accepted, but kept in mind when evaluating the results.

Initially, contact between the workpiece and the base plate was modelled by a rigid geometrical surface which is in frictional contact with the bottom of the workpiece. This surface is marked yellow in figure 4.2. The use of contact modelling in combination with fixed nodes resulted in significantly higher calculation times and convergence problems. More importantly, the resulting deformed shape contradicted the result of earlier calculations and practical tests, as can be seen in figure 4.3. Therefore, the contact between the workpiece plate and the base plate is not modelled in these simulations.

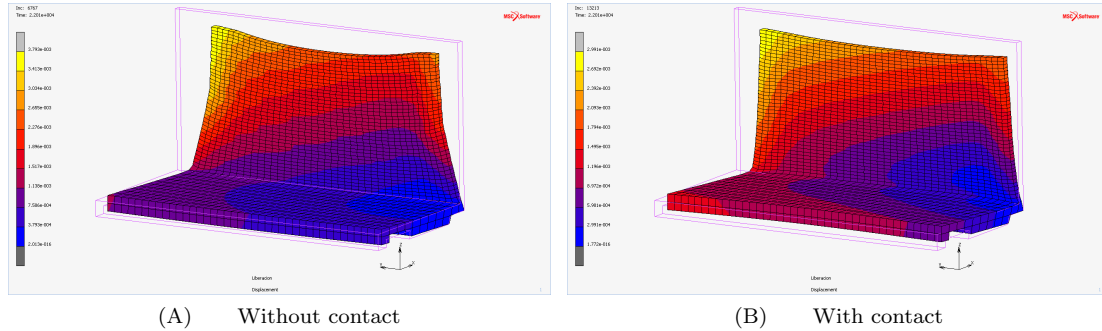


Figure 4.3: Comparison of the deformed shape after clamp release for the simple model with and without surface contact

The sum of the nodal reaction forces in (vertical) Z-direction over the dovetail surfaces are calculated for both the front (furthest from weld line) and middle (underneath weld line) dovetail. The largest reaction forces occur during the cooling phase, just before clamp release. Therefore all values are taken from this phase. The results are given in table 4.2. The values correspond to the order of magnitude that was expected from similar clamping situations for welding in literature [10]. Since there are no external forces in the final cooling phase, the sum of these reaction forces equals zero.

Location	Force
Front dovetail	-15.97 kN
Middle dovetail	15.97 kN

Table 4.2: Total reaction forces in Z-direction, simple model

4.2 Static structural analysis (estimation)

Instead of using fixed constraints in the dovetails, face foundations or springs are considered as well. According to literature[11] this gives more accurate results when modelling clamping. However, since the stiffness of the clamping structure is not known beforehand, an estimate of the has to be made first. For this purpose a static structural analysis of the clamping concept is done in ANSYS. Dimensions of the concept are determined in an iterative way, based on the forces calculated in section 4.1 and resulting stresses and deformations.

4.2.1 Geometry

For the geometry a CAD model of the final concept is used, which includes the workpiece plate and baseplate (both with dovetails), two wedges and a piston rod. The sharp edges of the moving piston part are filleted to prevent numerical singularities in these regions, since here the stress levels are expected to be critical. The model is imported in ANSYS and 1/9th of the total plate is isolated for analysis. This section includes all relevant parts and is representative for the rest of the plate assembly. Material properties of Ti6Al4V from literature[1] are again used for the workpiece plate. For the material of the clamping assembly, properties of standard structural steel are used. All parts of the resulting assembly are meshed as deformable. A refinement is applied to the top section of the piston, as critical stress levels are expected in this section. See figure 4.4 for the geometry and the resulting mesh.

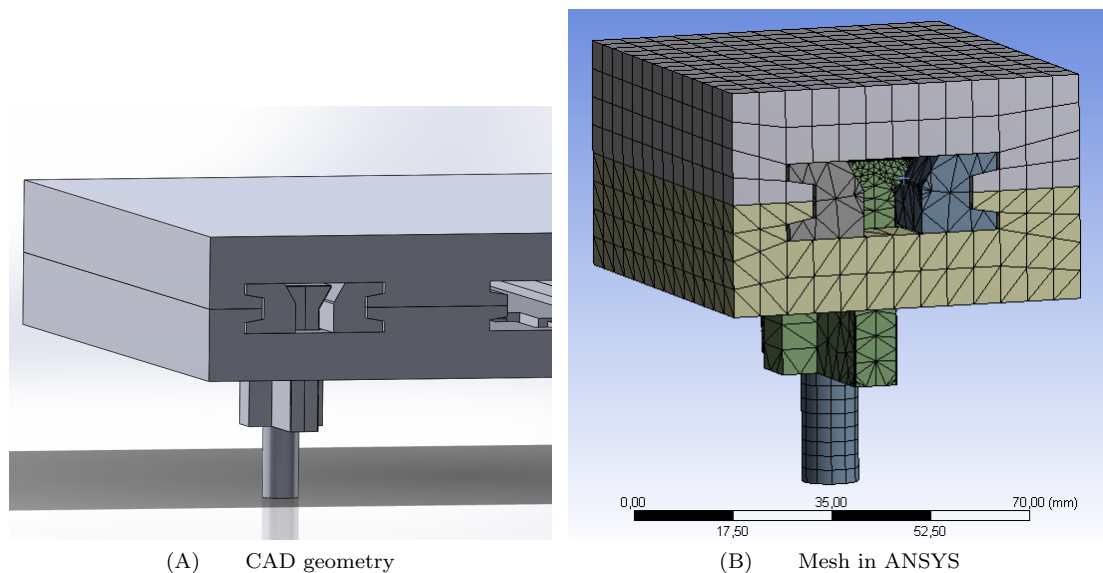


Figure 4.4: Geometry and mesh for static structural analysis

4.2.2 Method and results

The bottom of the baseplate is fixed in all direction, as it is connected to the fixed world at this point. The bottom of the cylinder part is also constrained because of the way the clamping load will be modelled. Finally, a translational joint is imposed on the cylinder in vertical direction. The rest of the model will be held in place by contact only and will not be constrained. As possible contact zones are modelled as frictional, except for the surfaces between the piston part and the baseplate that enable the vertical movement of the cylinder. These are modelled frictionless since they are not relevant for the solution. For the frictional contact pairs, a friction coefficient of 0.4 is assumed, based on internal research within Tecnalia. All contact pairs are modelled as asymmetric, which means that there is an explicit distinction between the contact surface and the target surface elements [12]. Typically, this results in the most accurate and efficient solution. Choices for contact and target bodies are made based on the ANSYS guidelines for contact faces [13]. Generally this comes down to the more convex body, or the body with the finest mesh, being the contact body. This results in the contact body definitions as stated in table 4.3.

Contact body	Target body
Piston	Wedge (x2)
Wedge (x2)	Workpiece plate
Wedge (x2)	Baseplate
Workpiece plate	Baseplate
Piston	Baseplate

Table 4.3: Contact and target body definitions in the ANSYS simulation

As there are corners and sharp edges in the contact regions, the default contact detection method of ANSYS, which is at the Gauss points of the elements, may cause convergence problems. Instead, *Nodal - normal to target* is used, which detects contact at a node where the normal direction is perpendicular to the surface of the target body.

The presence of contact regions in the analysis means that the problem is highly non-linear. This means that in ANSYS the Newton-Raphson method will be used to solve the problem. The convergence of this method depends particularly on the choice of time step[14]. A smaller time step means that the load is applied in more sub-steps, which aids convergence and results in a more accurate solution. However this comes at the cost of longer calculation times. To optimize this process, adaptive time stepping is used, which adjusts the time steps during the calculation run. Adaptive time stepping also introduces the bisection method. If at some point the program fails to reach convergence, the time step is cut in half and the program tries again from the last converged sub-step.

The simulation itself is carried out in two parts. In the first time step a pre-load is placed on the piston to simulate the clamping process. See the load labelled *B* in figure 4.5. This pushes the wedges outward which consequently clamps the workpiece to the baseplate. After the first time step the resulting displacement of the piston is locked to simulate a sufficiently large piston force. Consequently, in the second time step a load in vertical direction is placed on top of the workpiece plate to simulate the force due to thermal distortion. This is indicated by the load labelled *A* in figure 4.5. The magnitude of this load is derived from the results obtained from the simple model as given in table 4.2. After an iterative process of dimensioning, acceptable stresses and deformations are obtained. The resulting deformations in Z-direction are shown in figure 4.6A. The final obtained equivalent stresses are given in figure 4.6B. As can be seen in this figure, they are well below the yield strength of structural steel of 355 MPa.

The equivalent stiffness in Z-direction of the structure is calculated by using simply:

$$k_{eq} = \frac{F}{\Delta x}, \quad (4.5)$$

where Δx is the maximum deflection in vertical direction of the workpiece.

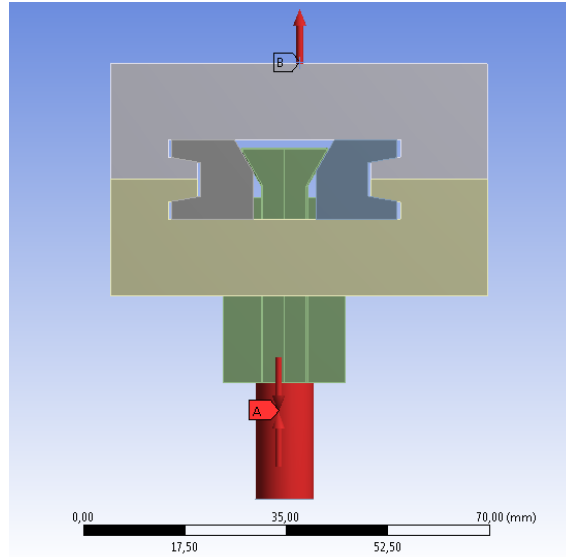


Figure 4.5: Applied forces in the static structural analysis in ANSYS

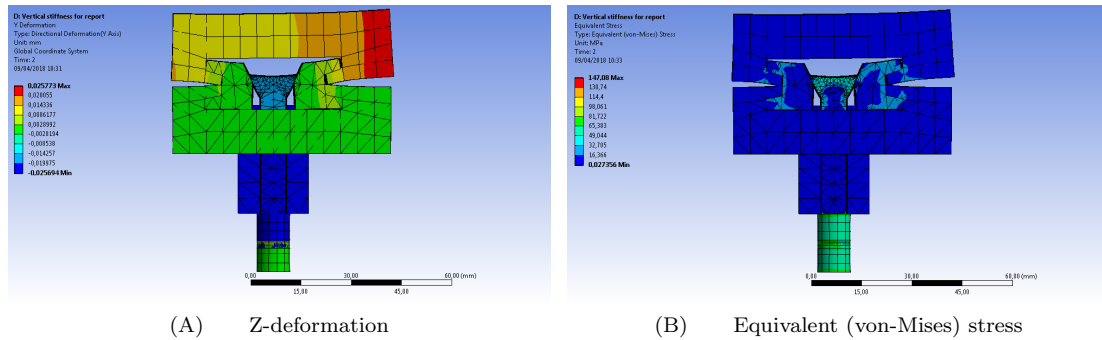


Figure 4.6: Z-deformation and equivalent stress results from the static structural analysis in ANSYS

4.3 Thermo-mechanical analysis (validation)

4.3.1 Springs

Method

In the model, spring elements are applied to the nodes inside the dovetail grooves, as shown in figure 4.7. Each spring element is connected to another node which is fixed in space, representing the connection to the ground. The stiffness per spring element is calculated by dividing the the total stiffness of the clamping structure as calculated with equation (4.5) by the number of springs. The springs are defined in such a way that they only act in the (vertical) global Z-direction. Note that this fixed degree of freedom differs from the *true direction* alternative, in which the spring force is collinear with the two nodes, regardless of their current orientation. To correspond with the actual clamping situation, the nodes inside the dovetail are fixed in X- and Y-direction.

Results

The final distorted shape after clamp release is shown in figure 4.8A. This shape is similar to the shape found with the simple clamped model, as shown in figure 4.3A, and also corresponds with practical tests. During the clamped phases there are some deflections in vertical direction, as shown in figure

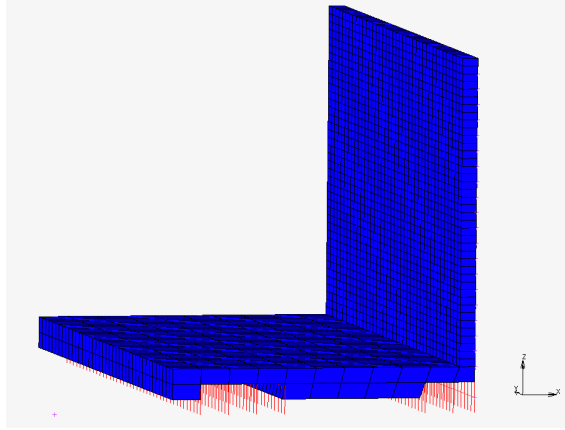


Figure 4.7: Simple model with the addition of springs in the dovetail sections

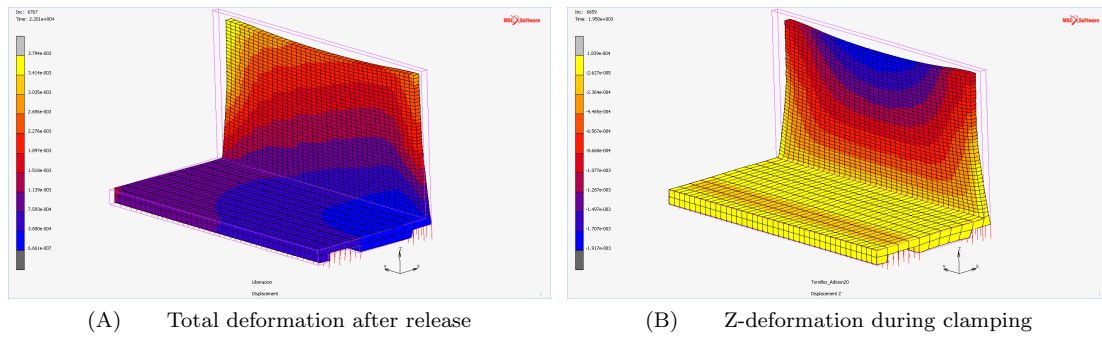


Figure 4.8: Scaled deformation of the simple model with springs

4.8B, indicating expected behaviour. However, in contrast to expectations, the reaction forces in vertical direction are in the same order of magnitude as the fully constrained model, which can be seen in table 4.4. If the fixed constraint in X- and Y-direction on the dovetail nodes is deactivated, reaction forces in Z-direction drop by two orders of magnitude. From this is concluded that more detailed analysis of effects in X- and y-direction is necessary.

Location	Force
Front dovetail	-15.94 kN
Middle dovetail	15.94 kN

Table 4.4: Total reaction forces in Z-direction, simple model

4.3.2 Detailed model

Method

Since the models from sections 4.1.2 and 4.3.1 did not provide satisfactory results, it is decided that a more accurate simulation is necessary. It is argued that the simple geometry of the initial analysis does not capture the behaviour of the clamped structure well enough to give any meaningful and sufficiently accurate results. Therefore a new model is built by meshing the conceptual geometry which was used earlier in the static structural analysis in section 4.2, including a separate body mesh for the baseplate. The resulting meshed model is shown in figure 4.9.

To this model, the same thermal conditions and welding paths are applied as to the simple model. For the baseplate a new material is defined based on stainless steel. Its material properties are temperature

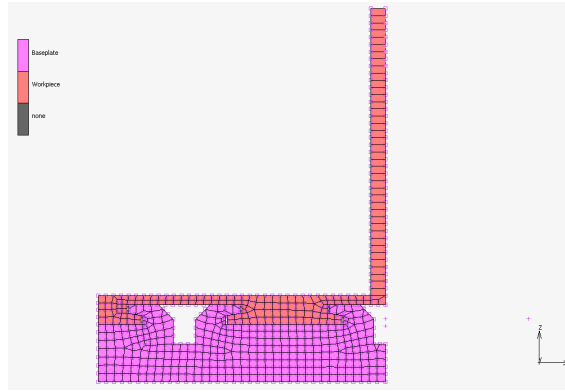


Figure 4.9: Detailed model based on the meshed conceptual design including baseplate.

dependant and can be found in literature[15, 16]. The exact values of these material properties can be found in appendix A.2. Instead of being fixed in space by fixed nodes or spring elements, the contact between the workpiece and the baseplate is used to geometrically lock the part using the shape of the dovetail. A contact between the two deformable bodies is defined using the *contact tables* option in Marc/Mentat. For the contact heat transfer coefficient a value of $2000 \text{ W/m}^2\text{K}$ is chosen, which is estimated based on heat transfer between steel and steel surfaces[17], since this is similar to the actual heat transfer between titanium alloy and steel. For the friction coefficient a value of 0.4 is used again. Both the baseplate and the workpiece are preheated prior to the start of the process. This is incorporated in the simulation by applying an initial temperature of 500 degrees Celsius to both of the parts.

For modelling the contact between the two bodies, two different methods are present in Marc/Mentat: node-to-segment and segment-to-segment contact [18]. Node-to-segment is the default option of Marc/Mentat and is as the name suggests based on contact of nodes with a segment, which can be a surface, element face or similar. Penetration is prevented using multi-point constraint equations. This way of applying constraints introduces a possible dependency on the choice of touching and touched bodies in the results. This problem is not present in the alternative option: segment-to-segment contact. Using this method, contact is detected between segments using auxiliary points located on each segment. With this method it is possible to show contact status on both sides of the contact interface and it generally results in a faster solution time. Therefore segment-to-segment contact is chosen for the analysis.

Results

Using the detailed model, results up to a job time of 100 seconds were obtained, which corresponds to the addition of one layer plus cooling time. However, running the entire simulation was estimated to take 30 days. Although the initial results appear to be realistic and reliable. It is decided to abort the simulation because of this long calculation time.

4.3.3 Detailed model with baseplate surface

Method

As an alternative for the completely meshed detailed model, a modified model was constructed in which the meshed baseplate was replaced by a rigid surface based on the same geometry. This new model is shown in figure 4.10.

The goal was minimizing calculation time, while not compromising too much on accuracy. For the contact modelling, the same definition is used as before. However, the value for the contact heat transfer coefficient cannot be left unchanged, since the geometrical surface does not have a thermal capacity or any other related thermal material properties. Due to limitations in MSC Marc/Mentat it is only possible to prescribe a time dependant temperature of the surface, but since the baseplate will also be cooling down during the process, this temperature profile is not known. As an alternative it is assumed that the

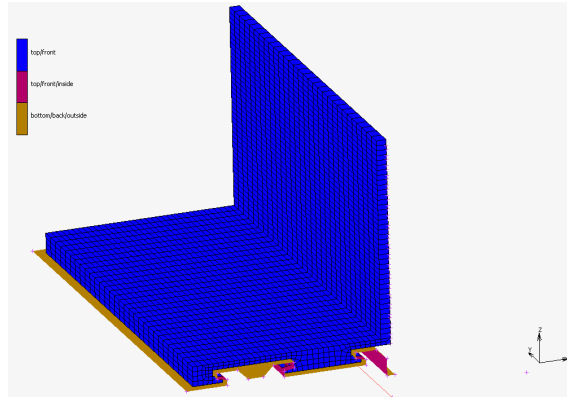


Figure 4.10: Detailed model based on the meshed conceptual design including rigid surface as baseplate

contact between workpiece and baseplate is insulated, and the coefficient of contact heat transfer is set to zero.

Due to limitations in the used version of MSC Marc/Mentat (2014.1.0), it was not possible to simulate contact release and unclamping at the end of the process. In order to obtain the final distorted shape, the analysis was repeated in the 2010 version of the program. The drawback of this solution is that node-to-segment contact had to be used. In the end values from the 2014 version simulation were used for post-processing, since these were reasoned to be more accurate. For the final deformation, results from the 2010 version were used, as this was the only possibility.

Results

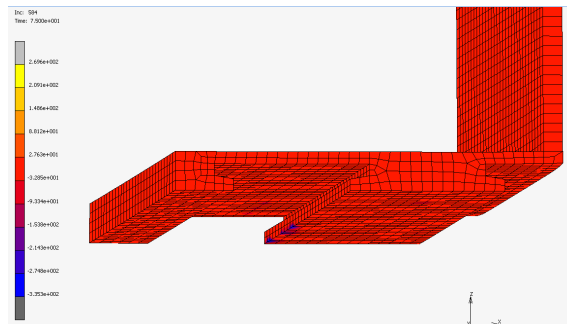


Figure 4.11: Outward normal reaction forces occurring in the wedged part of the dovetail (blue)

The first thing standing out when looking at the results is the presence of reaction forces in the contact areas. Note that in MSC Marc/Mentat there is a distinct difference between *reaction forces*, which are a result of constraining nodal degrees of freedom, and *contact forces*, which are a result of the program preventing penetration. Since there are no constraints at these nodes, in theory there should be no reaction forces. Having a closer look at the location of the reaction forces reveals that they mainly occur in the wedged part of the dovetail in the outward normal direction, as shown in figure 4.11. This leads to the conclusion that the forces are a result of the used contact algorithm, and can most likely be mapped as a contact normal force pointing inward on the other side of the wedge. This is confirmed by comparing the sum of the contact forces and reaction forces locally with the contact forces calculated by the node-to-segment method at the same nodes, because with this method the abnormal reaction forces were not present. These proved to be similar, so therefore it is concluded that the total forces acting on the geometry in a specific direction can be calculated as the sum of the directional contact normal forces, contact friction forces and reaction forces.

Comparing the results after the first 100 seconds with the detailed model with meshed deformable baseplate results in the values of table 4.5. As expected, the values are different, but the order of

magnitude and direction of the reaction forces are similar. Looking at the distribution of forces along the length of a dovetail in figure 4.12, it can be seen that the general shape is the same. This M-like distribution is typical for the residual stresses across a weld line[19, 20], which indicates that these results are accurate.

	Meshed	Surface
Front dovetail	-7.88 kN	-6.60 kN
Middle dovetail	7.88 kN	6.60 kN

Table 4.5: Comparison of contact forces in Z-direction between the detailed model with meshed deformable baseplate and rigid surface baseplate at time t=100s

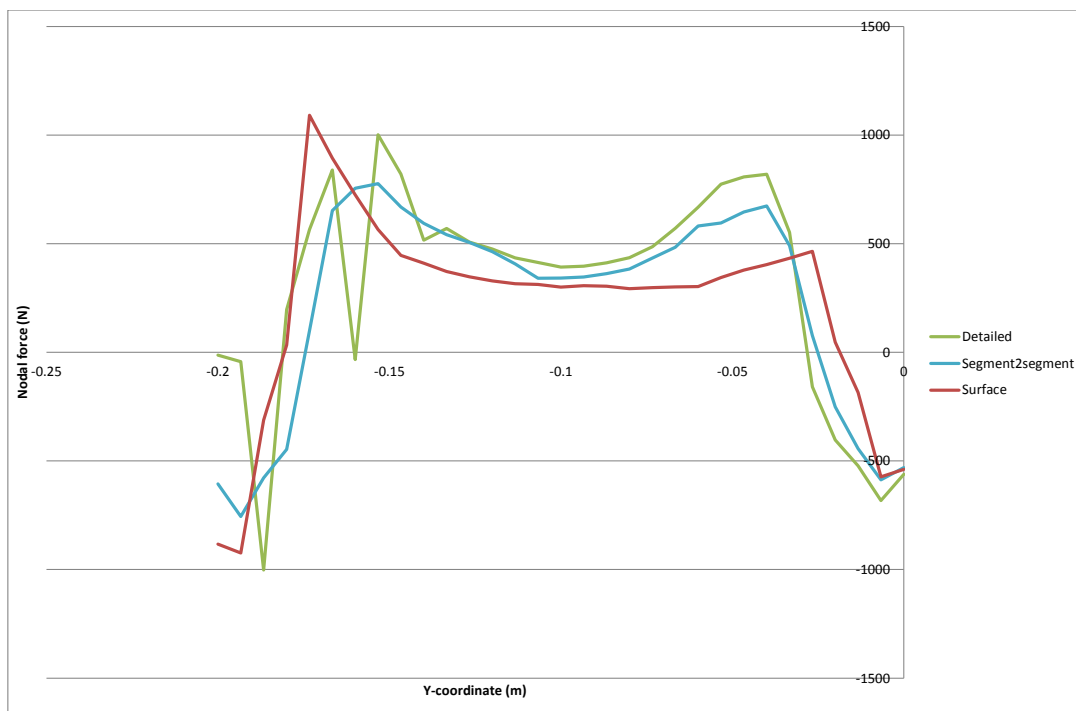


Figure 4.12: Comparison of the calculated reaction forces over the width of the dovetail of the detailed model, the detailed model with segment-to-segment contact and the detailed model with rigid surface baseplate

In order to find the maximum occurring vertical reaction force, a plot over time is made of these reaction forces. The values are calculated by taking the sum of the directional nodal forces in each of the dovetails, consisting of contact normal forces, contact friction forces and reaction forces. The resulting plot is shown in figure 4.13. In this graph, the addition of the separate layers can be clearly identified, as well as the final cooling down period to room temperature. The general shape of the graph can be explained by the changing stiffness of the structure due to the addition of the layers. The initial reaction forces are caused by the localized expansion of the workpiece as a result of welding. After the addition phase, the workpiece cools down, causing residual stresses, resulting in a change of direction of the reaction forces.

Figure 4.13B shows that the maximum reaction force $F_Z = 6.60kN$ occurs at t=100s, which is after the first cycle of addition and cooling down. The above procedure is repeated for the forces in X- and Y-direction, which results in maximum forces of $F_X = 109.08kN$ and $F_Y = 4.17kN$ respectively. Both occur at t=21,950s, which is after cooling down to room temperature and just before unclamping.

To obtain functional values of the “real” deformations after release, the following directional nodal deformations are measured along the three paths shown in figure 4.14:

- Z displacements along P1

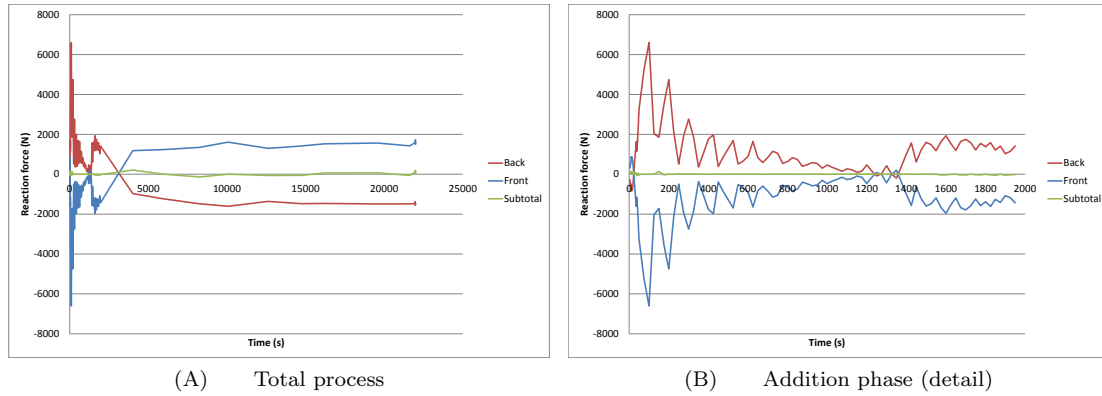


Figure 4.13: Reaction forces in Z-direction as function of time for both dovetails

- Y displacements along P2
- Z displacements along P3

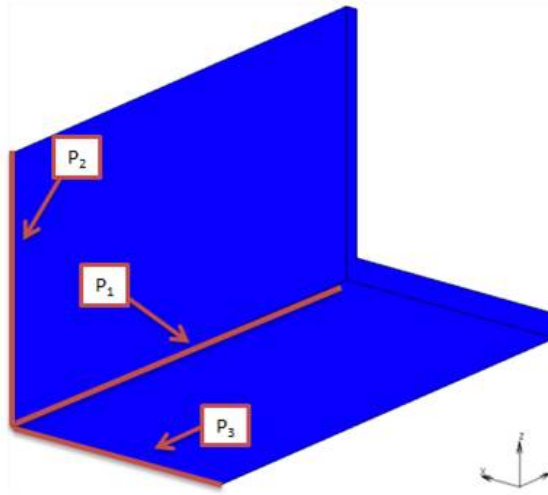


Figure 4.14: Paths used for calculation of the real deformation (source: internal Tecnia documentation)

Subsequently, the resulting path plots are transformed such that they represent the geometry resting on the ground (the line $Z=0$). The maximum value is then found to be the “real” deformation. This is illustrated with an example shown in figure 4.15. The resulting displacement values are shown in table 4.6. These values correspond with the order of magnitude that was expected from practical experiments and previous simulations using similar clamping schemes.

Path	Deformation (mm)
P1 (Z-deformation)	0.18
P2 (Y-deformation)	0.22
P3 (Z-deformation)	2.58

Table 4.6: Calculated “real” displacement values after clamp release

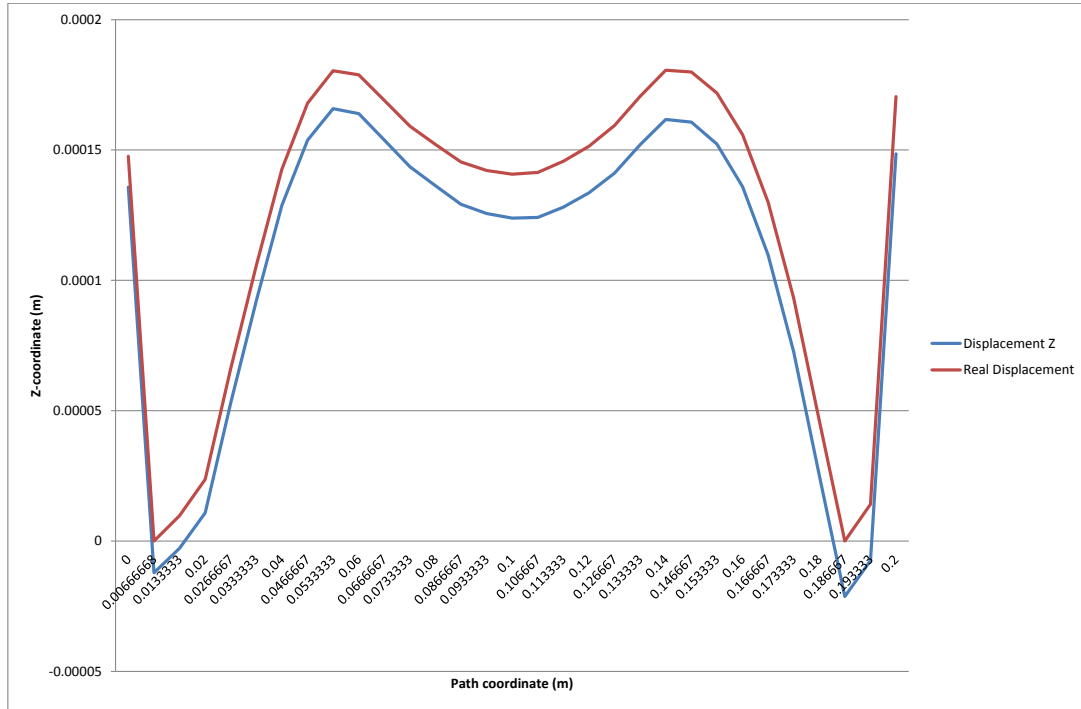


Figure 4.15: Measured Z-displacement and “real” displacement along P1

4.4 Static structural analysis (validation)

The results from section 4.3 clearly define two different loadcases for the structure. The first consists of the forces occurring in the front dovetail, which is the furthest from the weldline. Because of that, mainly forces in positive x- and z-direction are present. The other loadcase consists of the forces occurring in the middle dovetail, directly underneath the weldline. Because of the shrinkage of the plate, forces in both positive and negative x-direction occur here, and therefore the clamping system is loaded in compression. For each dovetail the “worst case” over time is selected. The resulting loadcases are summarized in table 4.7.

Axis	Front dovetail (t=21,950s)	Middle dovetail (t=100s)
X	36.36 kN	13.52 kN*
Y	4.17 kN	-1.33 kN
Z	523 N	2.20 kN

Table 4.7: Forces imposed on the workpiece plate for each loadcase.
* in compression

To ensure that the structure can withstand both of these loadcases, static structural analyses are done in ANSYS for both loadcases separately.

4.4.1 Geometry

The same geometry is used as defined in section 4.2.1. For the baseplate, the material properties of stainless steel are used as defined in section 4.3.2. For the wedges and piston AISI 4140 will be used, a commonly used high tensile steel. The thermal and elastic properties of structural steel are used in the simulation. Since critical parts are made with this material, the yield strength at elevated temperatures is an important property. From figure 4.16 can be concluded that $\sigma_y = 85ksi \approx 586MPa$ is an acceptable

estimate for the yield strength at a working temperature of 500 degrees Celsius, which is the temperature to which the baseplate and workpiece are preheated.

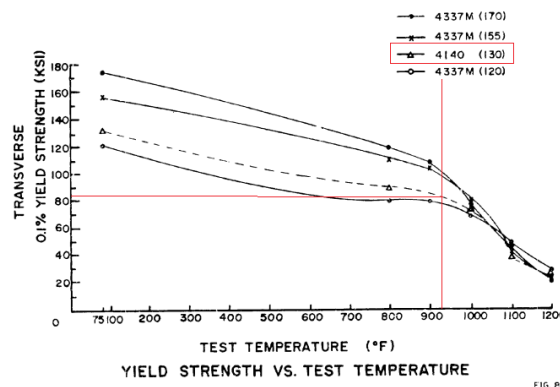


Figure 4.16: Yield strength vs. elevated test temperature for several low alloy steels [21]. Operating temperature and corresponding yield strength of the used material (AISI 4140 / 42CrMo4) are marked in red

For the dovetail under the weldline, shrinkage of the plate has to be modelled. For that reason, in the analysis of that loadcase the workpiece plate is split up in two parts and a pre-load is imposed between the two parts. This is shown in figure 4.17 by the location marked E. Between the two cut faces a translational boundary condition is imposed, which prevents the opposite faces from changing orientation with respect to each other. To prevent initial rigid body motion, sufficiently small forces are applied on both sides of the plate, marked B and C in figure 4.17.

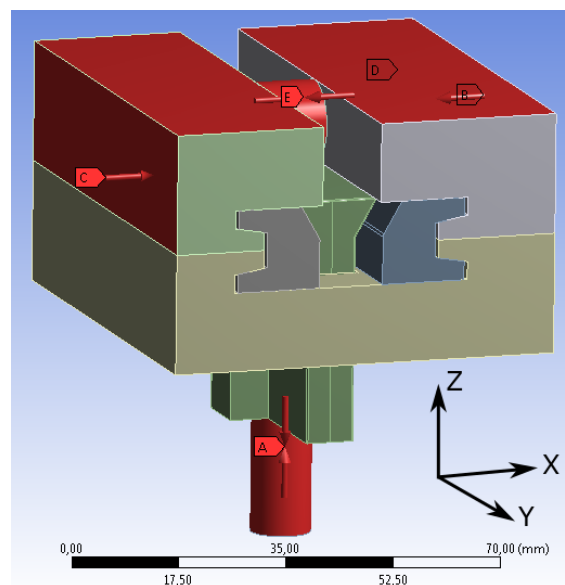


Figure 4.17: Geometry and applied forces of the loadcase analysing shrinkage of the workpiece

4.4.2 Method and results

Applying the loadcases as defined in table 4.7 to the clamping system results in the equivalent stress distributions as shown in figure 4.18. At the front dovetail, a peak stress of 579 MPa is visible. However, the location of this maximum value is in a know stress singularity point and is not critical to the solution. The highest occurring stress value in a non-singular location is 460 MPa, which is below the yield strength of AISI 4140 at 500 degrees Celsius, as determined in section 4.4.1. In the back dovetail loadcase, no relevant issues are found.

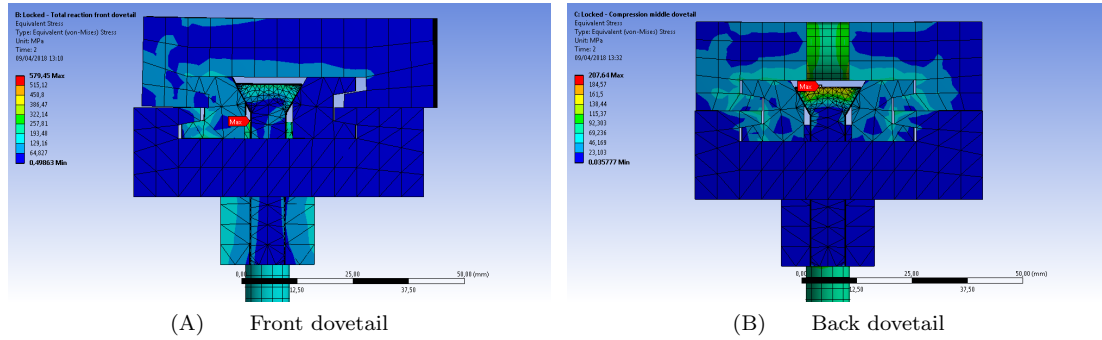


Figure 4.18: Equivalent (von-Mises) stress in the clamping structure for both loadcases

In section 4.2.2 the piston was assumed to be fixed during the loading phase, in order to determine the equivalent stiffness of the structure. For this analysis, initially the same boundary condition is applied. By determining the reaction forces in the piston during the process, a suitable value for the piston closing force will be obtained, based on which actuators will be selected. In table 4.8 the calculated values are displayed for both loadcases as defined in table 4.7. Note that these values are for 1/3 of the length of each dovetail. From this is concluded that the necessary actuator forces are unacceptable high, and a redesign is proposed.

Loadcase	Piston reaction force
Front dovetail	11,538 N
Back dovetail	6778 N

Table 4.8: Reaction forces during each loadcase in fixed piston

Chapter 5

Redesign

5.1 Design

Based on the simulation results in chapter 4 a redesign of the clamping system is proposed. The geometry is shown in figure 5.1 in both clamped and unclamped state. For this example, a clamped plate of 1x1m is assumed, to provide a generalisation of the solution. The connection with the table and the mechanical actuators including motor and transmission are also included. For the actuators and bevel gearboxes, representative CAD models from Kelston [22] are used, which will be further explained in section 5.3. A layer of insulation is indicated in light grey. With this redesign, vertical forces on the moving piston part are minimized. The design and components of the actual clamping mechanism are mostly the same as the final concept as described in section 3.3.2. The main difference is in the interaction between the piston and the two wedges, which is optimized with respect to geometrical space and force transmission. The interaction during the downwards clamping motion of the piston is now divided in two parts. In the first stage an contact angle of 45 degrees is used to push the wedges outwards into the dovetail, but not clamping them yet. In the second stage, the wide part of the piston is clamped between the two wedges using a 2 degree contact angle. This is shown in figure 5.1C. Because the contact plane between the piston and the wedges is located lower, a v-shaped slot is added to the baseplate. In the clamped position, the prismatic shape fits in the slot. This also prevents the actuator from being pushed down too far as a result of reaction forces.

The motion for unclamping is largely the same as in the system before redesign. A protruding edge from the piston is inserted into the angled grooves of the wedges, pushing them inside with the upward motion of the piston. The dimensions are chosen in such a way that in the most upward position, the wide part of the piston fits exactly between the two wedges, as shown in figure 5.1D. To accommodate for this system, while still being able to retract the wedges in such a way that there is enough clearance to remove the plate vertically, the width of the dovetail groove had to be increased from 40 mm to 50 mm. As still more than 15 mm of material is left between each of the dovetails, it is reasoned that this is a modification without consequences to the structural strength of the construction.

In appendix B, technical drawings of the clamping system applied to a 200x200mm test set-up are given.

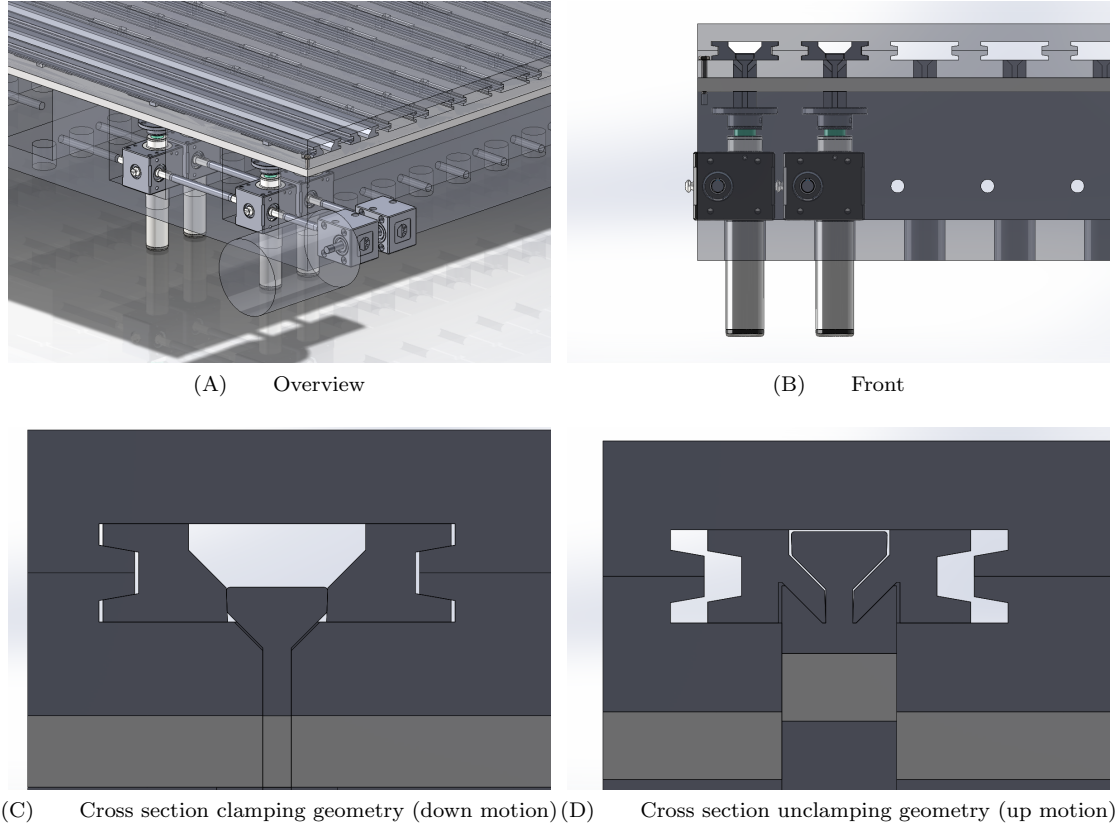


Figure 5.1: Redesign applied to 1x1m plate

5.2 Validation

The loadcase calculations of section 4.4 are repeated with the new geometry. The imposed boundary conditions are unchanged. However, using the same method resulted in convergence issues due to penetration and sudden contact changes affecting the force balance. To prevent this, the contact normal stiffness factor between the piston part and the wedges is modified to 0.1, which changes the normal stiffness to 10% of its default value. In the same contact areas, the detection method is changed to *Nodal - Projected Normal From Contact*, which sets the detection location to the overlapping region of contact and target surfaces [13]. The advantage of using this projection based method in this case is that gap and penetration are averaged over the detection region, resulting in smoother penalty loads and contact pressures when there are sudden contact status changes.

After simulation, the results are checked for too much penetration and incorrect changes of contact status, both of which were not present. The resulting reaction forces in the piston are given in table 5.1. Note that the occurring reaction forces are negative in this case, which means that during the process the piston is not loaded in positive vertical direction. Therefore, no continuous actuating forces are necessary in the redesign. The v-shaped slot mentioned in section 5.1 fixes the piston under the load of these reaction forces.

Loadcase	Piston reaction force
Front dovetail	-827 N
Back dovetail	-3702 N

Table 5.1: Reaction forces during each loadcase in fixed piston

In reality the piston will not be fixed in the second load-stage. For that reason the analysis is repeated, such that realistic (piston) stresses and displacements will be obtained. Instead of a fixed boundary condition, a sufficiently large constant load is applied to the bottom of the piston. All other conditions are left the same. The resulting equivalent stress distributions for the front and back dovetail loadcases are shown in figure 5.2 and 5.3 respectively.

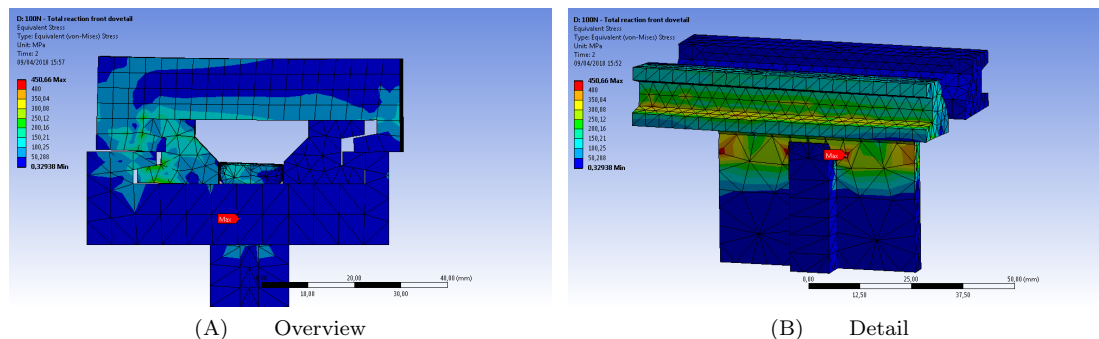


Figure 5.2: Equivalent (von-Mises) stress in the redesigned clamping structure for the front dovetail loadcase

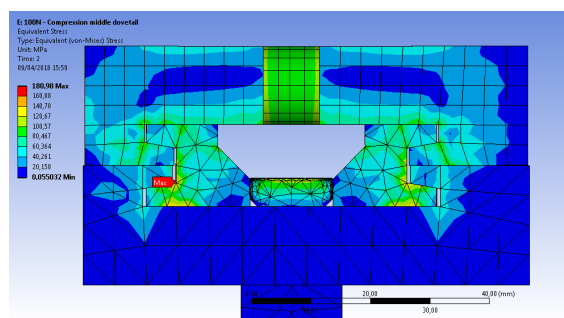
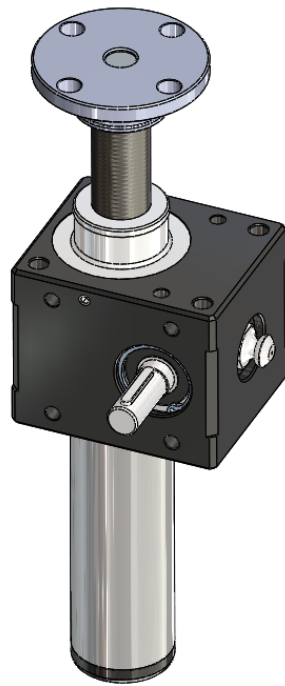


Figure 5.3: Equivalent (von-Mises) stress in the redesigned clamping structure for the back dovetail loadcase

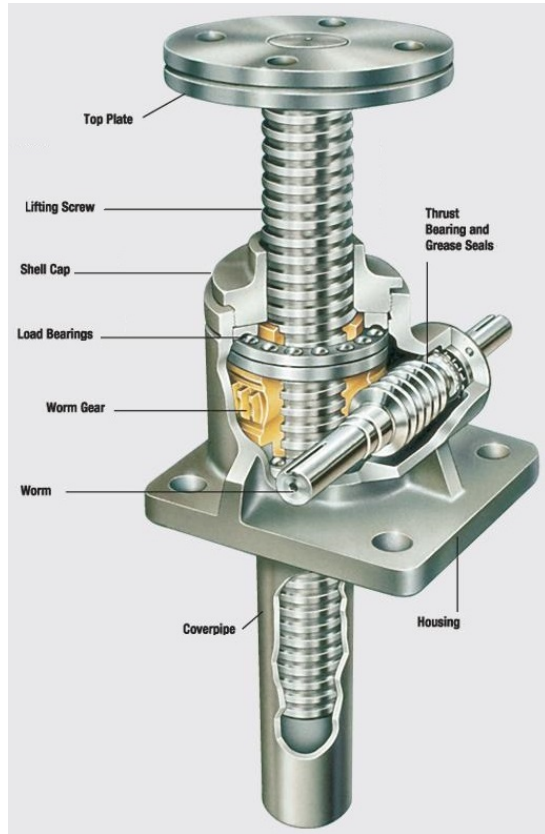
For clarity, a detailed view of the front dovetail loadcase is included in figure 5.2B, such that the location of the maximum stress is made visible. Since in this loadcase the loads are mostly in positive X-direction, the maximum is located at the thinnest section of the piston part, as a result of bending. The maximum stress value of 451 MPa is sufficiently below the yield strength to be considered safe. The maximum stress of the back dovetail loadcase is located on the inside edge of one of the wedges. Although this is a critical part and location, the value of 181 MPa is reasoned to be sufficiently low to not cause problems.

5.3 Actuators

As stated in section 3.3.3, a choice is made to use electro-mechanical actuators for the clamping system. Since holding forces during clamping are minimized with the redesign, forces required to unclamp the wedges are expected to be the determining factor in the dimensioning of the actuators. These are not yet known at the time of writing, since practical tests have to be conducted first. To still provide a complete overview of the entire system, a provisional choice is made for a commercial solution: the Kelston CM25-T-100-0025N-F mini cubic screw jack actuator [22]. A technical datasheet can be found in appendix C. This actuator fits within the given dimensions and can provide 2.5 kN of lifting force. In figure 5.4 the CAD model of the actuator is displayed next to a cut drawing of a comparable system showing the working principle. A large advantage of this specific solution is the possibility to interconnect the actuators in series and/or parallel, such that only one electrical motor is needed. In figure 5.5, some typical system arrangements are given. The resulting actuator layout which is included in the design can be seen in figure 5.1A.



(A) CAD model [22]



(B) Working principle [23]

Figure 5.4: Mechanical screw jack actuator

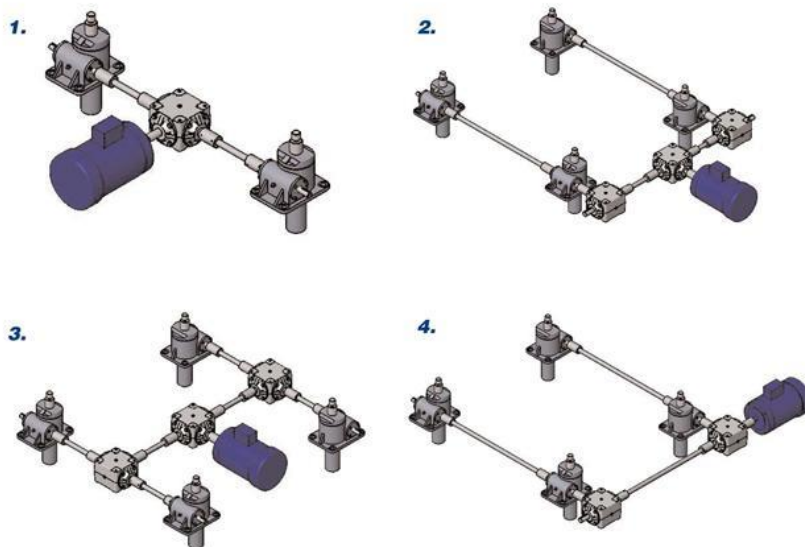


Figure 5.5: Some typical system arrangements in which actuators are interconnected [23]

Chapter 6

Conclusion

The goal of this study was to design and validate a universal clamping system, which constrains the workpiece during material addition and does not require significant changes in the product design. Based on this principle, several concepts are created. After internal discussion and a comparison of advantages and disadvantages, a final concept is chosen and further developed.

Using coupled thermo-mechanical FEM analyses, knowledge of the WAAM process was obtained and reaction forces were determined. Subsequent static structural FEM analyses were used in dimensioning and validation of the design. From this, the final design solution is proposed, which satisfies the set requirements and withstands the occurring loads during the process. Although the clamping system is developed for the 200x200mm test set-up, it is designed in such a way that it's modular and is applicable to a substrate plate of arbitrary dimensions. The resulting simulated distortions after release correspond with expectations from practical experiments and previous simulations using similar clamping schemes.

6.1 Future work

Because of limited availability of the WAAM equipment, practical tests could not be conducted yet within Tecnia, which is the current limitation to this research. Because of this reason, practical tests fall outside the scope of this report. Previous comparisons between practical tests and simulation results showed great promise for the use of FEM simulation in describing the WAAM process effectively and in the prediction of final distortions and residual stresses. However, it is a highly non-linear process with many relevant parameters and is therefore difficult to model. For that reason, practical tests are essential to validate the obtained results.

At the time of writing, future research including these practical tests is planned within Tecnia. Instead of implementing the entire clamping system at once, first the working principle will be tested by constraining the workpiece with an abundant amount of screws. In contrast to the conventional clamping method, these screws will be inserted into machined holes in the bottom of the plate, such that constraints can be applied under the weldline, in accordance with the actual design. If these tests confirm the expected results and result in a reduction of distortions, a test set-up of the design will be constructed and implemented in the tests. Instead of using electrical motors to drive the mechanical actuators, it is recommended to operate the actuators manually in the test set-up.

If the design proves to be effective during real life tests, distortions will be mitigated in WAAM manufactured products. This is expected to aid the commercial adoption of this technology and make it a more viable alternative to conventional machining.

Bibliography

- [1] J Ding. Thermo-mechanical analysis of wire and arc additive manufacturing process. 2012.
- [2] Jing Guo, Yong Zhou, Changmeng Liu, Qianru Wu, Xianping Chen, and Jiping Lu. Wire arc additive manufacturing of az31 magnesium alloy: Grain refinement by adjusting pulse frequency. *Materials*, 9(10):823, 2016.
- [3] T Artaza, A Alberdi, M Murua, J Gorrotxategi, J Frías, G Puertas, MA Melchor, D Mugica, and A Suárez. Design and integration of waam technology and in situ monitoring system in a gantry machine. *Procedia Manufacturing*, 13:778–785, 2017.
- [4] H Vallejo, M Seco, Z Yousaf, and I Garmendia. Contributions from simulation to the improvement of the waam process. 2017.
- [5] James M Gere and S Timoshenko. *Mechanics of materials*. 2001.
- [6] Warren Clarence Young and Richard Gordon Budynas. *Roark's formulas for stress and strain*, volume 7. McGraw-Hill New York, 2002.
- [7] Filippo Montevercchi, Giuseppe Venturini, Antonio Scippa, and Gianni Campatelli. Finite element modelling of wire-arc-additive-manufacturing process. *Procedia CIRP*, 55:109–114, 2016.
- [8] John A Goldak and Mehdi Akhlaghi. Computer simulation of welding processes. *Computational Welding Mechanics*, pages 16–69, 2005.
- [9] John Goldak, Aditya Chakravarti, and Malcolm Bibby. A new finite element model for welding heat sources. *Metallurgical transactions B*, 15(2):299–305, 1984.
- [10] Muhammad Abdul Wahab, MS Alam, MJ Painter, and PE Stafford. Experimental and numerical simulation of restraining forces in gas metal arc welded joints. *WELDING JOURNAL-NEW YORK*, 85(2):35, 2006.
- [11] Tobias Schenk. Modelling of welding distortion; the influence of clamping and sequencing. 2011.
- [12] David H Johnson. Principles of simulating contact between parts using ansys. In *Penn State-Erie, Erie, Pennsylvania, USA. 2002 International ANSYS Conference*, 2002.
- [13] ANSYS Guide. Ansys structural analysis guide. 2015.
- [14] Klaus Jürgen Bathe and Arthur P Cimento. Some practical procedures for the solution of nonlinear finite element equations. *Computer methods in applied mechanics and engineering*, 22(1):59–85, 1980.
- [15] Lu Zhang and P Michaleris. Investigation of lagrangian and eulerian finite element methods for modeling the laser forming process. *Finite elements in analysis and design*, 40(4):383–405, 2004.
- [16] British Stainless Steel Association et al. Elevated temperature physical properties of stainless steels, 2016.
- [17] Theodore L Bergman and Frank P Incropera. *Fundamentals of heat and mass transfer*. John Wiley & Sons, 2011.
- [18] MSC Marc. Volume a: Theory and user information. *MSC Software Corporation*, 2000.

- [19] C Dalle Donne, E Lima, J Wegener, A Pyszalla, and T Buslaps. Investigations on residual stresses in friction stir welds. 2001.
- [20] Caterina Casavola, Alberto Cazzato, Vincenzo Moramarco, and Carmine Pappalettere. Influence of the clamps configuration on residual stresses field in friction stir welding process. *The Journal of Strain Analysis for Engineering Design*, 50(4):232–242, 2015.
- [21] Richard S DeFries. The elevated temperature properties of two 81mm mortar tube alloys 4337m and 4140. Technical report, WATERVLIET ARSENAL NY, 1971.
- [22] Kelston. Screw jacks, actuators, gearboxes and jacking systems. <https://www.kelstonactuation.com/>. Accessed: 2018-03-27.
- [23] Duff-Norton. Machine screw actuators. <https://www.duffnorton.com/machine-screw-actuators-additional-information>. Accessed: 2018-03-14.

Appendix A

Material properties

A.1 Ti6Al4V

T [°C]	E [Pa]
20	$1.18 \cdot 10^{11}$
200	$1.02 \cdot 10^{11}$
400	$8.70 \cdot 10^{10}$
500	$7.50 \cdot 10^{10}$
600	$5.30 \cdot 10^{10}$
700	$4.00 \cdot 10^{10}$
800	$3.50 \cdot 10^{10}$
1600	$3.50 \cdot 10^{10}$

Table A.1: Young's modulus at elevated temperatures

T [°C]	ν
20	$3.30 \cdot 10^{-1}$
2800	$3.30 \cdot 10^{-1}$

Table A.2: Poisson's ratio at elevated temperatures

T [°C]	σ_{yield} base [Pa]	σ_{yield} filler [Pa]
20	$9.80 \cdot 10^8$	$7.84 \cdot 10^8$
93	$8.20 \cdot 10^8$	$6.56 \cdot 10^8$
205	$7.10 \cdot 10^8$	$5.68 \cdot 10^8$
315	$6.00 \cdot 10^8$	$4.80 \cdot 10^8$
425	$5.70 \cdot 10^8$	$4.56 \cdot 10^8$
540	$4.00 \cdot 10^8$	$3.20 \cdot 10^8$
600	$3.00 \cdot 10^8$	$2.40 \cdot 10^8$
700	$1.30 \cdot 10^8$	$1.04 \cdot 10^8$
800	$4.00 \cdot 10^7$	$3.20 \cdot 10^7$

Table A.3: Yield strength at elevated temperatures

T [°C]	CTE [1/K]
20	$9.00 \cdot 10^{-6}$
650	$9.70 \cdot 10^{-6}$
1600	$1.08 \cdot 10^{-5}$

Table A.4: Coefficient of thermal expansion at elevated temperatures

T [°C]	κ [W/mK]
20	7.00
300	$1.00 \cdot 10^1$
600	$1.40 \cdot 10^1$
900	$2.00 \cdot 10^1$
1200	$2.20 \cdot 10^1$
1500	$2.50 \cdot 10^1$
1600	$2.60 \cdot 10^1$
1660	$3.40 \cdot 10^1$
3000	$3.40 \cdot 10^1$

Table A.5: Thermal conductivity at elevated temperatures

T [°C]	cp [J/kgK]
20	$5.50 \cdot 10^2$
300	$6.00 \cdot 10^2$
600	$6.70 \cdot 10^2$
900	$7.30 \cdot 10^2$
1200	$6.70 \cdot 10^2$
1500	$7.10 \cdot 10^2$
1600	$7.30 \cdot 10^2$
1660	$8.40 \cdot 10^2$
3000	$8.40 \cdot 10^2$

Table A.6: Specific heat at elevated temperatures

A.2 Stainless steel

T [°C]	E [Pa]
20	$2.00 \cdot 10^{11}$
100	$1.94 \cdot 10^{11}$
200	$1.86 \cdot 10^{11}$
300	$1.79 \cdot 10^{11}$
400	$1.72 \cdot 10^{11}$
500	$1.65 \cdot 10^{11}$
600	$6.00 \cdot 10^{10}$
700	$4.00 \cdot 10^{10}$
800	$3.00 \cdot 10^{10}$
900	$2.00 \cdot 10^{10}$
1000	$1.00 \cdot 10^{10}$
5000	$1.00 \cdot 10^{10}$

Table A.7: Young's modulus at elevated temperatures

T [°C]	ν
20	$2.93 \cdot 10^{-1}$
100	$3.11 \cdot 10^{-1}$
200	$3.30 \cdot 10^{-1}$
300	$3.49 \cdot 10^{-1}$
400	$3.67 \cdot 10^{-1}$
500	$3.86 \cdot 10^{-1}$
600	$4.05 \cdot 10^{-1}$
700	$4.23 \cdot 10^{-1}$
800	$4.42 \cdot 10^{-1}$
900	$4.61 \cdot 10^{-1}$
1000	$4.80 \cdot 10^{-1}$
2000	$4.80 \cdot 10^{-1}$

Table A.8: Poisson's ratio at elevated temperatures

T [°C]	σ_{yield} [Pa]
20	$2.40 \cdot 10^8$
205	$1.60 \cdot 10^8$
316	$1.34 \cdot 10^8$
427	$1.14 \cdot 10^8$
538	$9.70 \cdot 10^7$
649	$8.80 \cdot 10^7$
760	$7.60 \cdot 10^7$
1500	$1.50 \cdot 10^7$
2000	$1.50 \cdot 10^7$

Table A.9: Yield stress at elevated temperatures

T [°C]	CTE [1/K]
20	$1.60 \cdot 10^{-5}$
100	$1.60 \cdot 10^{-5}$
200	$1.65 \cdot 10^{-5}$
300	$1.70 \cdot 10^{-5}$
400	$1.75 \cdot 10^{-5}$
500	$1.80 \cdot 10^{-5}$
2000	$1.80 \cdot 10^{-5}$

Table A.10: Coefficient of thermal expansion at elevated temperatures

T [°C]	κ [W/mK]
20	$1.50 \cdot 10^1$
1400	$3.35 \cdot 10^1$
2000	$3.35 \cdot 10^1$

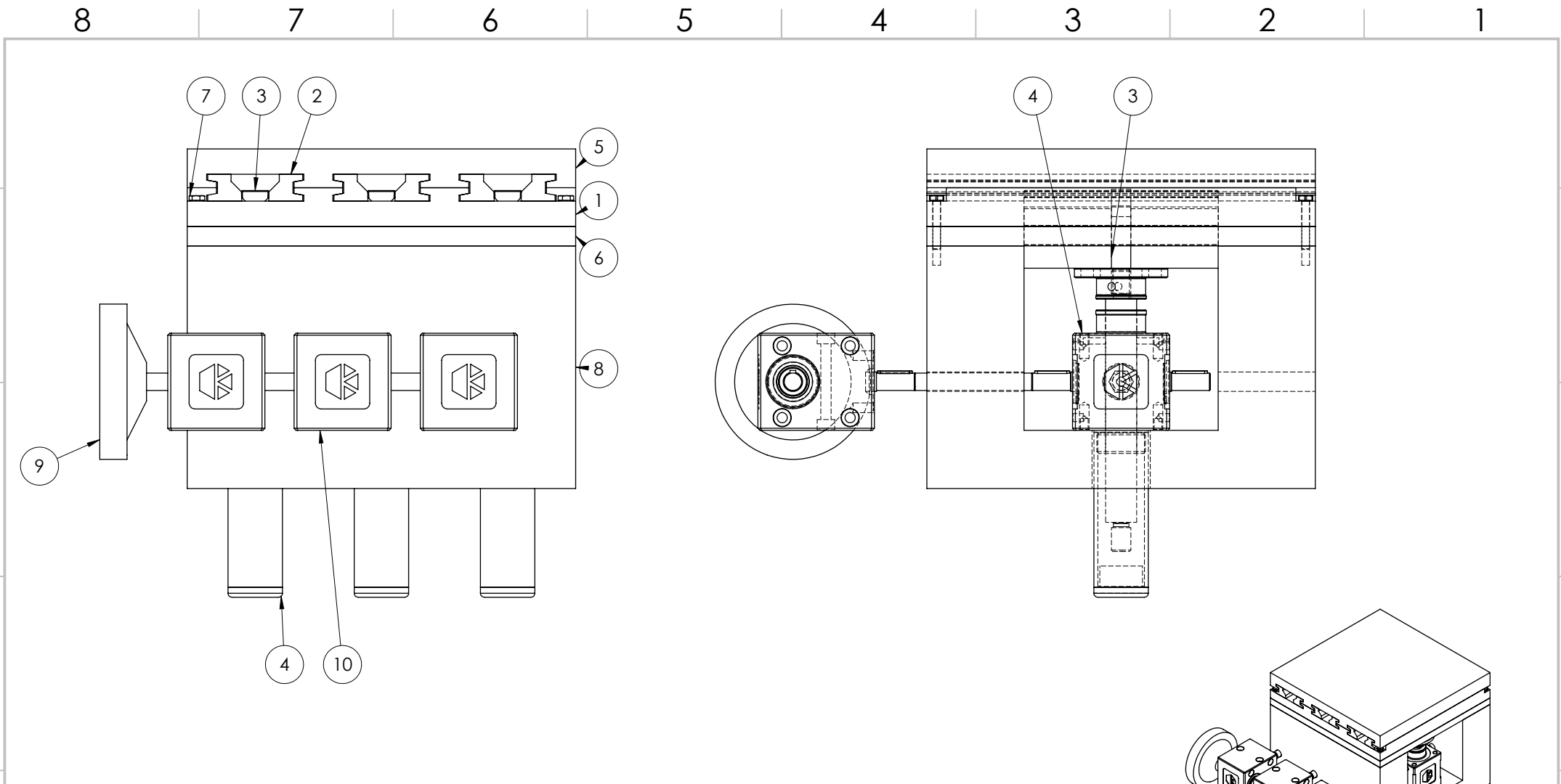
Table A.11: Thermal conductivity at elevated temperatures

T [°C]	cp [J/kgK]
20	$5.00 \cdot 10^2$
200	$5.00 \cdot 10^2$
700	$6.00 \cdot 10^2$
2000	$6.00 \cdot 10^2$

Table A.12: Specific heat at elevated temperatures

Appendix B

Technical drawings



ITEM NO.	PART NUMBER	DESCRIPTION	QTY.
1	baseplate		1
2	wedge		6
3	piston_assembly		3
4	Kelston_CM25-T-0025		3
5	plate_dovetail		1
6	insulation_plate		1
7	ISO 4014 - M4 x 25 x 14-N		4
8	table		1
9	wheel		1
10	bevel_gearbox		3

UNLESS OTHERWISE SPECIFIED: DIMENSIONS ARE IN MILLIMETERS		FINISH:	DEBURR AND BREAK SHARP EDGES		DO NOT SCALE DRAWING	REVISION
SURFACE FINISH:						
TOLERANCES:						
LINEAR:						
ANGULAR:						
DRAWN	NAME	SIGNATURE	DATE	TITLE:		
CHK'D						
APPV'D						
MFG						
Q.A						
				MATERIAL:		
				WEIGHT:		
				DWG NO.	A3	
				clamped_plate		
				SCALE:1:2	SHEET 1 OF 1	

4

3

2

1

F

F

E

E

D

D

C

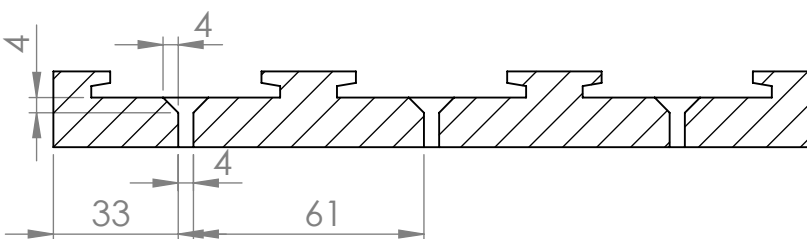
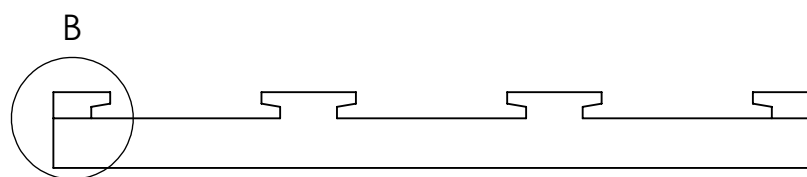
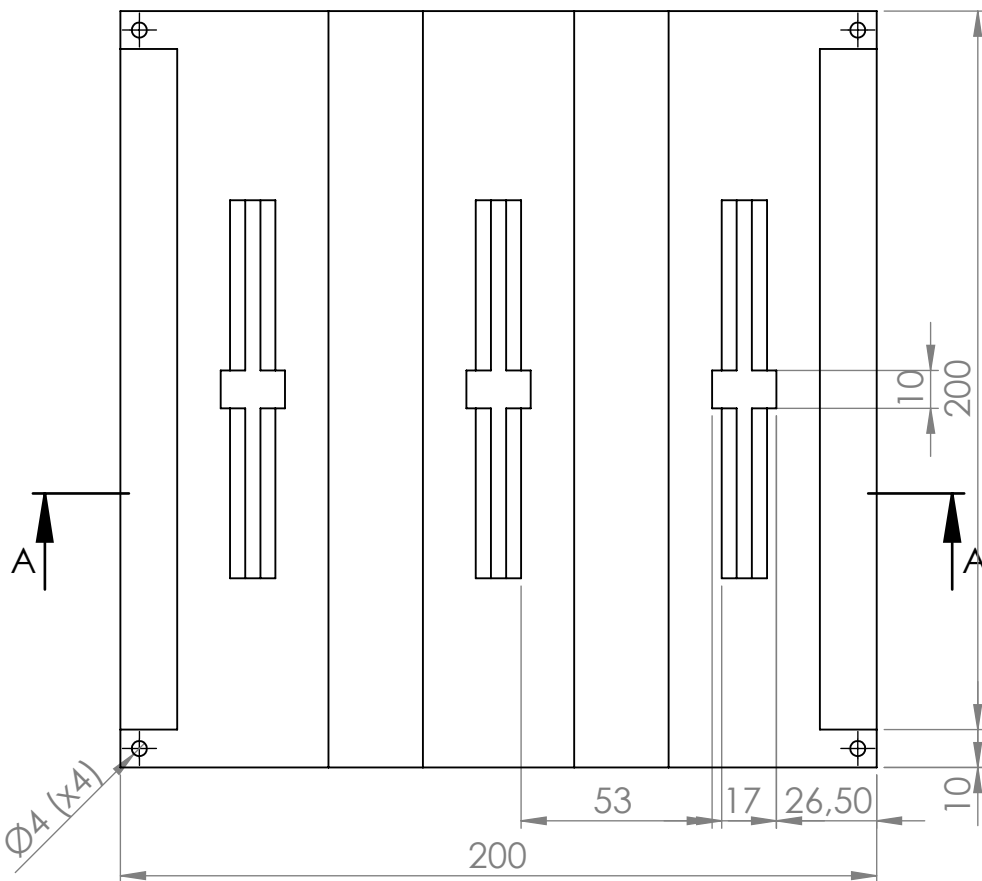
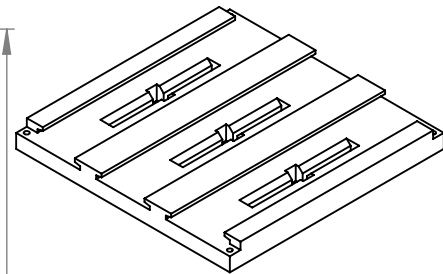
C

B

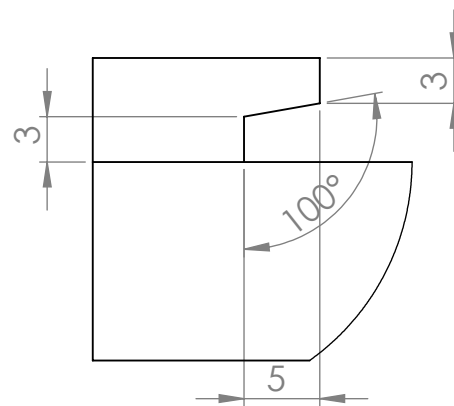
B

A

A



SECTION A-A



DETAIL B
SCALE 2 : 1

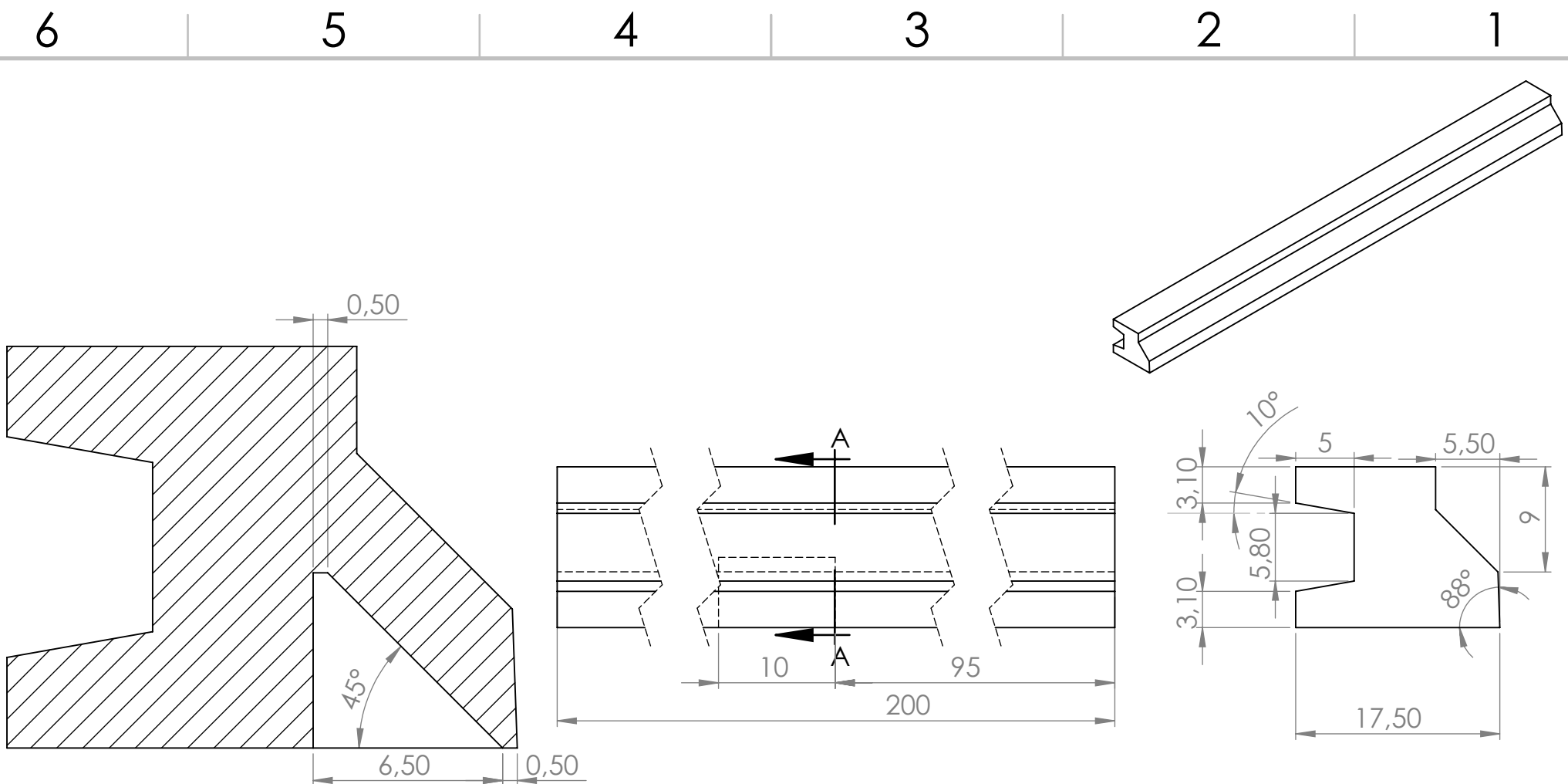
UNLESS OTHERWISE SPECIFIED: DIMENSIONS ARE IN MILLIMETERS SURFACE FINISH: TOLERANCES: LINEAR: ANGULAR:			FINISH:		DEBURR AND BREAK SHARP EDGES		DO NOT SCALE DRAWING		REVISION	
DRAWN			SIGNATURE		DATE		TITLE:			
CHK'D										
APPV'D										
MFG										
Q.A					MATERIAL:		DWG NO.		A4	
							baseplate			
					WEIGHT:		SCALE:1:2		SHEET 1 OF 1	

4

3

2

1



SECTION A-A
SCALE 5 : 1

UNLESS OTHERWISE SPECIFIED: DIMENSIONS ARE IN MILLIMETERS SURFACE FINISH: TOLERANCES: LINEAR: ANGULAR:				FINISH:		DEBURR AND BREAK SHARP EDGES		DO NOT SCALE DRAWING		REVISION	
DRAWN				SIGNATURE		DATE		TITLE:			
CHK'D											
APPV'D											
MFG											
Q.A						MATERIAL:		DWG NO.		A4	
								wedge			
						WEIGHT:		SCALE:2:1		SHEET 1 OF 1	

6 5 4 3 2 1

D

C

B

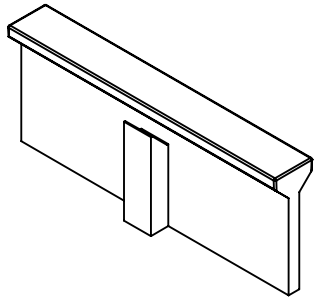
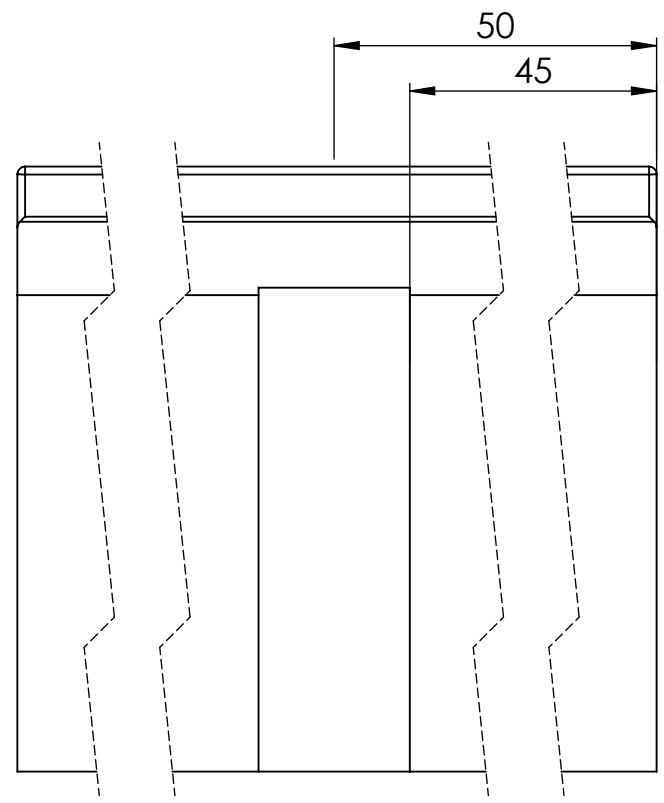
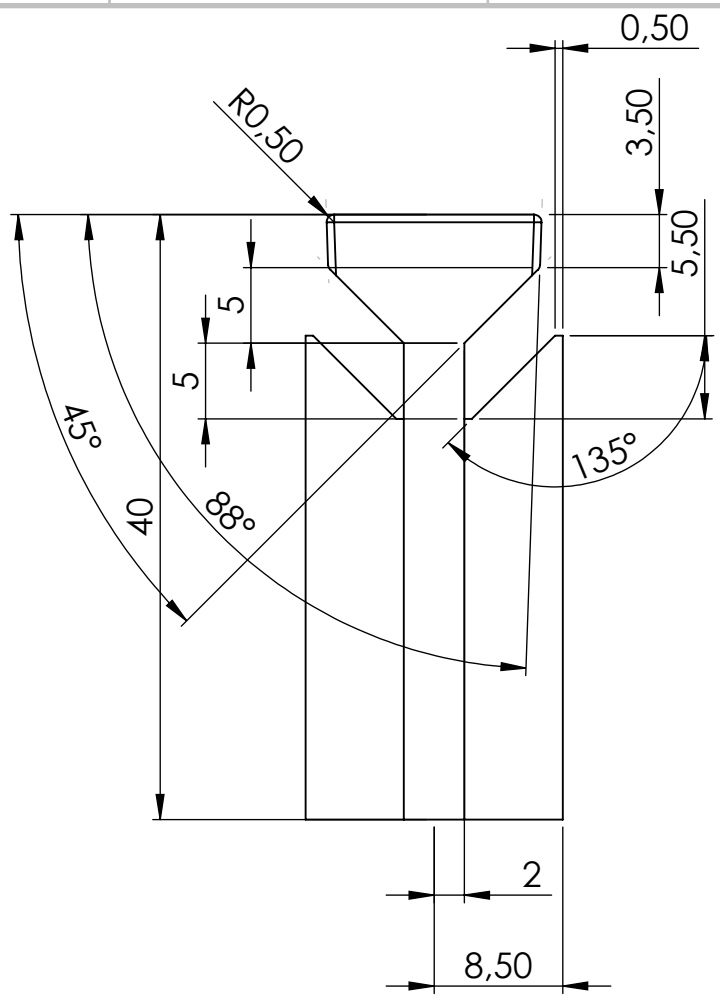
A

D

C

B

A



UNLESS OTHERWISE SPECIFIED: DIMENSIONS ARE IN MILLIMETERS SURFACE FINISH: TOLERANCES: LINEAR: ANGULAR:				FINISH:		DEBURR AND BREAK SHARP EDGES		DO NOT SCALE DRAWING		REVISION	
DRAWN				SIGNATURE		DATE		TITLE:			
CHK'D											
APPV'D											
MFG											
Q.A						MATERIAL:		DWG NO.			
								piston_clamp			
						WEIGHT:		SCALE:2:1		SHEET 1 OF 1	

6 5 4 3 2 1

4

3

2

1

F

F

E

E

D

D

C

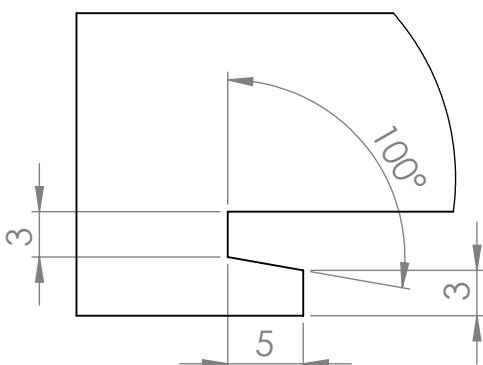
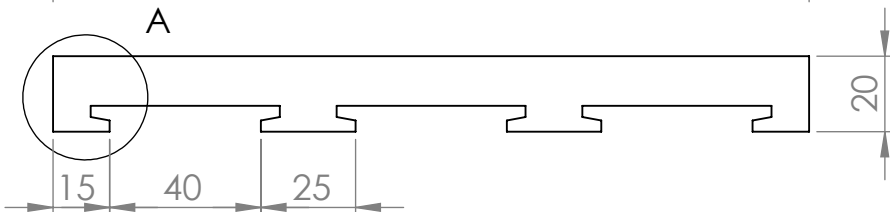
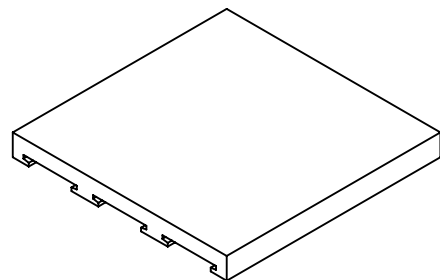
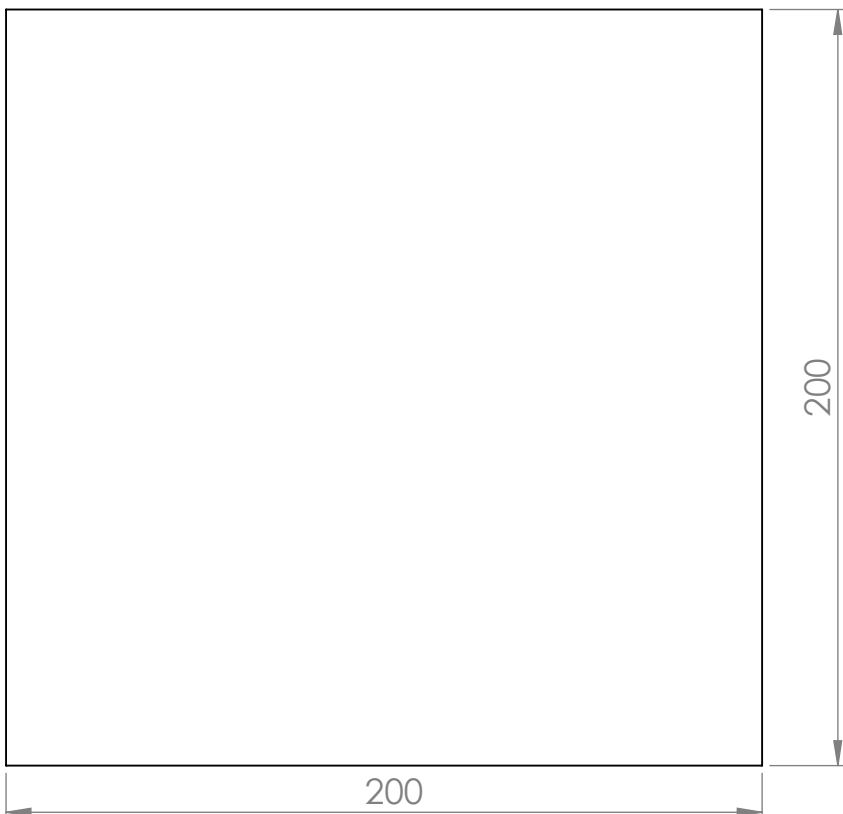
C

B

B

A

A



DETAIL A
SCALE 2 : 1

UNLESS OTHERWISE SPECIFIED: DIMENSIONS ARE IN MILLIMETERS SURFACE FINISH: TOLERANCES: LINEAR: ANGULAR:			FINISH:		DEBURR AND BREAK SHARP EDGES		DO NOT SCALE DRAWING		REVISION	
DRAWN			SIGNATURE		DATE		TITLE:			
CHK'D										
APPV'D										
MFG										
Q.A					MATERIAL:		DWG NO.		A4	
							plate_dovetail			
					WEIGHT:		SCALE:1:2		SHEET 1 OF 1	

4

3

2

1

4

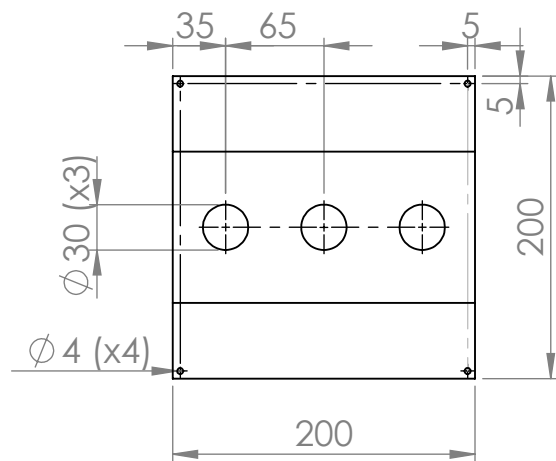
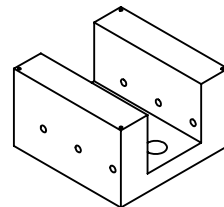
3

2

1

F

F

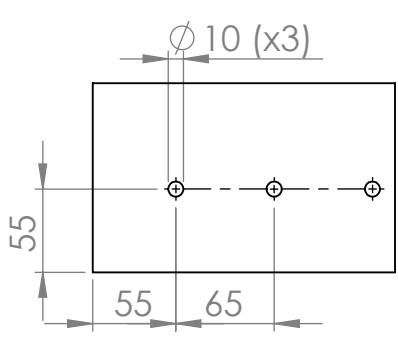


E

E

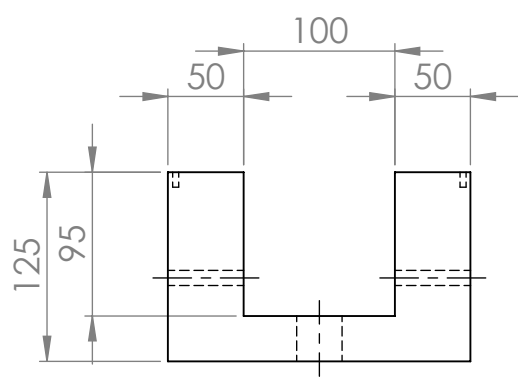
D

D



C

C



B

B

UNLESS OTHERWISE SPECIFIED: DIMENSIONS ARE IN MILLIMETERS SURFACE FINISH: TOLERANCES: LINEAR: ANGULAR:			FINISH:		DEBURR AND BREAK SHARP EDGES		DO NOT SCALE DRAWING		REVISION		
DRAWN			SIGNATURE		DATE		TITLE:				
CHK'D											
APPV'D											
MFG											
Q.A							MATERIAL:		DWG NO.		A4
									table		
							WEIGHT:		SCALE:1:5		SHEET 1 OF 1

A

A

4

3

2

1

Appendix C

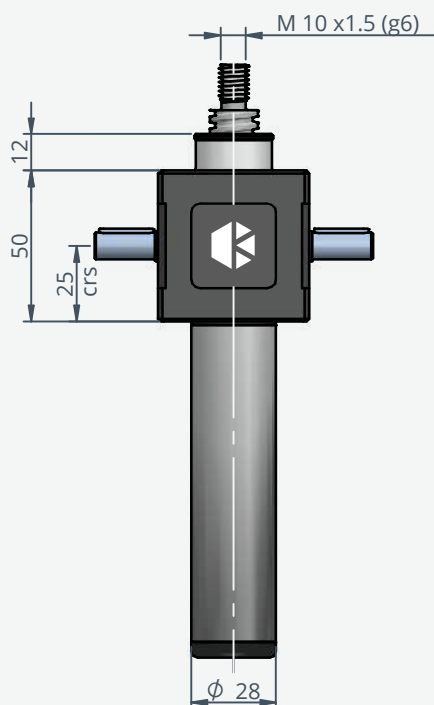
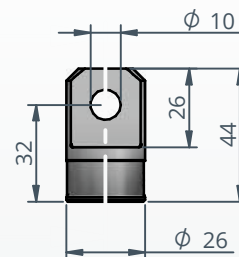
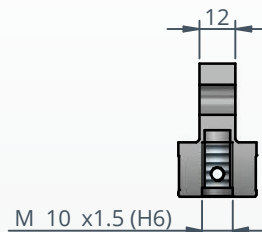
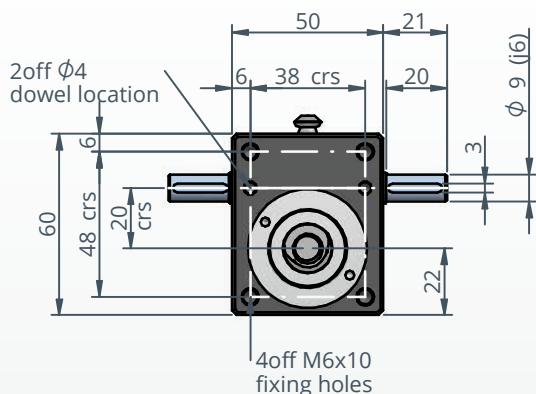
Screw jack datasheet

Mini Cubic Screw Jack

CM25 Translating screw

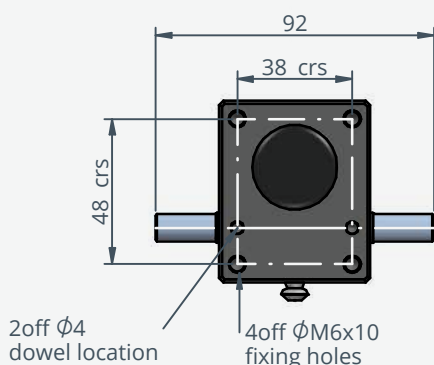
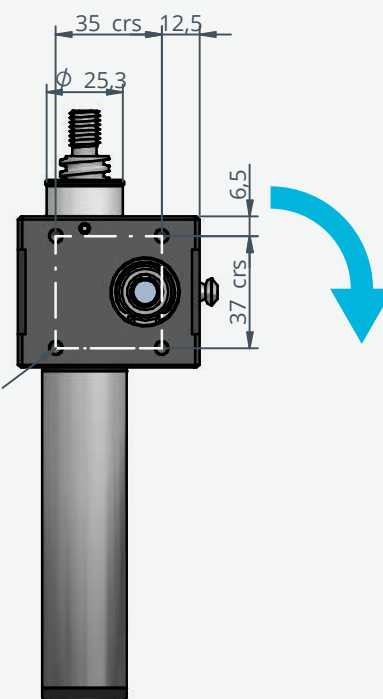
2.5kN

nominal capacity



↑
Rotation to
lift load

4 off M5x5
fixing holes
each side



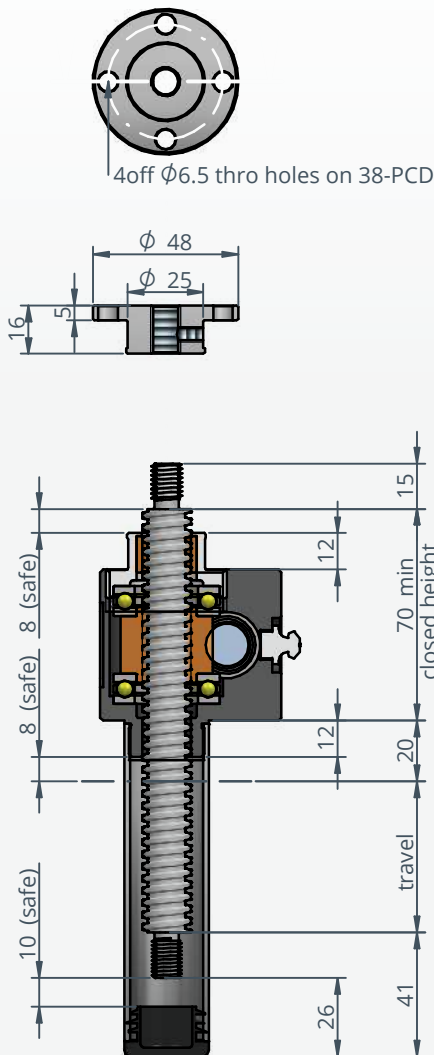
CM25 Technical data

	High ratio / single start trapazoidal	High ratio / double start trapazoidal	Low ratio / single start trapazoidal	Low ratio / double start trapazoidal
Travel rate of wormshaft (mm/rev)	0.25	0.5	1.0	2.0
Worm gear ratio	16:1	16:1	4:1	4:1
Lifting screw diameter (mm)	Tr 16x4	Tr 16x8	Tr 16x4	Tr 16x8
Pitch (mm)	4.0	4.0	4.0	4.0
Lead (mm)	4.0	8.0	4.0	8.0
Root diameter (mm)	12.5	12.5	12.5	12.5
Input torque required to lift 2.5kN	0.43Nm	0.63Nm	1.19Nm	1.77Nm

SHEET 1 OF 2

Mini Cubic Screw Jack

CM25 Translating screw



CM25	T	***	****	*
Screw jack model	Translating screw	Travel speed	Length of travel	End fitting

Precision machined 6082T6 aluminium body, manufactured from a solid billet.

Nickel plated, steel end caps and screw covers with stainless steel keys and fasteners further enhance corrosion resistance.

Designed for the adjustment of process equipment and systems.

Mounting

The screw jack body is provided with threaded mounting holes and dowel location holes on both mounting faces allowing the screw jack to be mounting in an upright or inverted position.

Gearset

Precision ground wormshaft, paired with a CA104 aluminium bronze wormwheel for added durability, supported by quality bearings and seals.

CM25 Linear Travel Speed mm/min				
Rotation speed of wormshaft rpm	Travel rate mm/rev			
	0.25	0.5	1.0	2.0
50	12.5	25	50	100
100	25	50	100	200
200	50	100	200	400
300	75	150	300	600
400	100	200	400	800
500	125	250	500	1000

